$3.00

NASA CONTRACTOR REPORT

NASA CR-2260

NASA CR-2260

DESIGN AND DEVELOPMENT OF THE SPINNING MODE SYNTHESIZER

by John M. Seiner and Gerhard Reethof

Prepared by
PENNSYLVANIA STATE UNIVERSITY
University Park, Pa. 16802
for Langley Research Center

NATIONAL AERONAUTICS AND SPACE ADMINISTRATION • WASHINGTON, D. C. • APRIL 1973

1. Report No.	2. Government Accession No.	3. Recipient's Catalog No.
NASA CR-2260		

4. Title and Subtitle	5. Report Date
DESIGN AND DEVELOPMENT OF THE SPINNING MODE SYNTHESIZER	April 1973
	6. Performing Organization Code

7. Author(s)	8. Performing Organization Report No.
John M. Seiner and Gerhard Reethof	
	10. Work Unit No.

9. Performing Organization Name and Address	11. Contract or Grant No.
Acoustics and Noise Control Laboratory Pennsylvania State University University Park, PA 16802	NGL 39-009-121
	13. Type of Report and Period Covered
12. Sponsoring Agency Name and Address	Contractor Report
National Aeronautics and Space Administration Washington, DC 20546	14. Sponsoring Agency Code

15. Supplementary Notes

16. Abstract

The purpose of this research has been to design and develop a flexible source of spinning modes which is capable of generating independent spinning waves of controlled complexity and spin speed without the introduction of broad band elements. These features were accomplished through the use of eight commercial loudspeakers located in an equally spaced circular array with diameter of 11 inches and properly phased so that the system could generate a spinning wave. The constructed apparatus was tested in an anechoic environment and found capable of generating a plane, one and two lobed spinning wave of high quality with a sound pressure level of 120 dB and at frequencies ranging from 1500 to 2500 Hz at a distance of 4 ft in the far field. The wave speeds investigated varied from 8000 to 18000 rad/sec which represent supersonic peripheral speeds.

17. Key Words (Suggested by Author(s))	18. Distribution Statement
Noise Source Spinning Modes Duct Acoustics Fan Noise	Unclassified - Unlimited

19. Security Classif. (of this report)	20. Security Classif. (of this page)	21. No. of Pages	22. Price*
Unclassified	Unclassified	56	$3.00

*For sale by the National Technical Information Service, Springfield, Virginia 22151

Page Intentionally Left Blank

TABLE OF CONTENTS

SUMMARY

The purpose of this research has been to design and develop a flexible source of spinning modes which is capable of generating independent spinning waves of controlled complexity and spin speed without the introduction of broad band elements. These features were accomplished through the use of eight commercial loudspeakers located in an equally spaced circular array with diameter of 11 inches and properly phased so that the system could generate a spinning wave. The constructed apparatus was tested in an anechoic environment and found capable of generating a plane, one and two lobed spinning wave of high quality with a sound pressure level of 120 dB and at frequencies ranging from 1500 to 2500 Hz at a distance of 4' in the far field. The wave speeds investigated varied from 8000 to 18000 rad/sec which represent supersonic peripheral speeds.

INTRODUCTION

Today it is the accepted belief that the periodic redistribution of pressure over the profile of fan or compressor rotor blades as they intersect the wakes of upstream objects can give rise to the phenomenon of propagating spiral waves. In the past, research on developing an effective and economical design for attenuating these spiral waves by absorption and cut-off techniques has been frustrated by the presence of a severely inhomogeneous turbulent velocity and temperature spectra through which the wave must propagate. In particular, those studies directed toward relating pertinent properties of duct lining configurations operating in a jet engine service environment are further complicated by the presence of a multitude of these spiral waves along with a high level of background broadband noise. In general, the duct geometry is highly complex and sound levels are sufficiently high to warrant the need for using the nonlinear wave equation to describe propagation.

Thus the possibility for a meaningful parameter variation that could lead to a more fundamental understanding of the characteristics of propagating spiral waves in actual turbomachinery applications is limited. Hence, there has arisen a genuine need for the development of a flexible and predictable source of spinning waves so that the pertinent parameters characterizing their propagation can be more easily related to absorption properties of various configurations of different lining materials. In addition, the propagating characteristics of spinning waves in ducts of varying cross sections is an area of considerable interest and could be studied more effectively. The objective of this research was the design and development of such a device.

THE ANALYSIS

WAVEFORMS TO BE SYNTHESIZED

As a first approximation we shall assume that the propagating waveform can be described by linear acoustics. Therefore, away from the source region the complex wave structure of these spinning waves may be effectively synthesized by a linear combination of normal modes each of which satisfy the homogenous wave equation and prescribed boundary conditions. The selection of the boundary conditions ultimately fixes the form of the normal modes as well as the eigenvalues in the expansion. Thus selection of the boundary conditions determines the form of the proposed Spinning Mode Synthesizer.

In order to select an economical and representative design, we chose for the boundary conditions a straight, hard-walled concentric cylindrical duct terminated anechoically. This permits the use of boundary conditions describing an infinite duct, or that of acoustic waves propagating in one direction only. The purpose for doing this is that the forcing function in the non-homogenous wave equation only serves to specify the numerical values of the Fourier components in the eigenfunction expansion. The composite form of these Fourier amplitudes will depend upon the particular engine design. To date, there has thus far been no adequate analytical treatment for evaluation of these coefficients, and until there is, one must rely upon experimental measurements. But, as will become clear later, it is always possible to adjust the amplitude and phase of these components to any desired level. Hence, we seek only to develop a device capable of generating individually the discrete set of eigenfunctions that could contain propagating acoustic energy in the duct of a rotor. We are now in position to investigate the form of the discrete set of eigenfunctions that are allowed subject to the above assumptions.

ALLOWED COMPRESSOR MODES

The first penetrating analysis on the form of the permitted normal modes and the criterion for their propagation or decay in terms of pertinent compressor variables was presented in Tyler and Sofrin's [1] classic paper on "Axial Flow Compressor Noise".[1] Basically, they obtained their result by analyzing the acoustic field away from the source region. It was, therefore, possible to use the standard technique of separation of variables to the homogenous wave equation with the previously mentioned boundary conditions. This permitted a solution for the form of the eigenfunctions that could be used in a Fourier synthesis of the sound field. Their result is presented as equation (1), and the coordinate system is defined in Figure 1.

$$P(r,\theta,Z,t) = \sum_{n=0}^{\infty} \sum_{m=-\infty}^{\infty} [A_{mn} \cos(m\theta - \omega t + \phi_{mn}] \times \left[\sum_{\mu=0}^{\infty} E^{\sigma}_{m\mu} (k^{\sigma}_{m\mu} r)\, e^{ik_z Z} \right] \qquad (1)$$

[1] References are given in the Bibliography.

where

$$E^{\sigma}_{m\mu}\ (k^{\sigma}_{m\mu} r) = J_m\ (k^{\sigma}_{m\mu} r) - \frac{J_m'\ (\sigma b k^{\sigma}_{m\mu})}{Y_m'\ (\sigma b k^{\sigma}_{m\mu})}\ {}^{*}Y_m\ (k^{\sigma}_{m\mu} r)$$

and

J_m, Y_m	are cylindrical Bessel and Newman functions respectively
$k^{\sigma}_{m\mu}$, m, k_z, ω	are eigenvalues of the (r, θ, Z, t) coordinates respectively
A_{mn}, ϕ_{mn}	are amplitude and phase coefficients of the mnth wave
μ	radial mode index
σ	hub-tip ratio (a/b)
m	circumferential mode index
n	harmonic of blade passage frequency

where primes indicate the first derivative with respect to r.

In order to determine the specific form of the eigenvalues, the boundary conditions must be applied. However, since only three of the eigenvalues are independent, Tyler and Sofrin chose the Z coordinate eigenvalue to be represented in terms of the characteristic time and radial modes

$$k_z = [(\frac{\omega}{c})^2 - (k^{\sigma}_{m\mu})^2]^{1/2} \qquad (2)$$

The radial boundary condition for a hard-walled duct requires that

$$(\frac{\partial P}{\partial r})_{a,b} \equiv 0$$

and application of these boundary conditions force $k^{\sigma}_{m\mu}$ to satisfy the relation

$$J_m'\ (bk^{\sigma}_{m\mu})\ Y_m'\ (\sigma bk^{\sigma}_{m\mu}) - J_m'\ (\sigma bk^{\sigma}_{m\mu})\ Y_m'\ (bk^{\sigma}_{m\mu}) = 0 \qquad (3)$$

In their analysis Tyler and Sofrin do not describe how one is to obtain the (θ,t) eigenvalues. In order to satisfy the solution of the equation, the allowed order of circumferential modes can be shown to be given by equation (4).

$$m = n B + h V \tag{4}$$

The reader is referred to Appendix B, where a derivation is given for obtaining such a relation. Since the interaction frequency $(nB\Omega)^{-1}$ is available for forming a characteristic time it is reasonable to assume that $\omega = nB\Omega$.

In their paper, Tyler and Sofrin present an excellent discussion of why sound modes of increasing complexity, increased waviness, are subject to decay in the duct and why lower order modes can propagate without decay. The condition when $\frac{\omega}{c} = k_{m\mu}$ is known as duct cut-off. This condition is reached by essentially considering whether the value of k_z is real or imaginary in equation 1. Decay occurs when k_z is imaginary, and it can be shown from equations 2 and 3 that this tends to be the case when m and μ increase in value. Thus it appears that the most fundamentally important modes to investigate from the standpoint of unattenuated propagation would be that of lowest order. We have adopted this procedure in the design of the experimental apparatus by limiting the number of sound sources in the final array.

It is worthwhile to remember that equation 1 only serves as a model for structuring the sound pressure distribution in actual turbomachinery applications. One must eventually take into account the inlet flow as well as the duct's finite length and termination geometry. Since precise specification of the rotor field's acoustic source distribution is still not possible, the spectral energy level and distribution in wavenumber space for propagating duct modes remains difficult to relate to various aerodynamic variables. Therefore in the development of the synthesizer we would have to assure that all propagating modes contain an equal amount of acoustic energy. This restriction gives rise to the design criterion that the geometrical configuration of the proposed device should produce the flattest possible output spectrum in wavenumber space.

Thus in an attempt to provide a greater flexibility for the synthesizer, the sound pressure field in a semi-infinite duct terminated at one end was computed for a source ring distribution as shown in Figure 2. The details of this calculation are given in Appendix C and the results of this calculation (Equation C.6) is reproduced here as equation 5. As one can observe

$$P(\underline{x},t) = \frac{\varepsilon_m k \rho c Q}{2\pi b^2} \frac{\cos(m\theta+\phi m)\, J_m(k_{m\mu} r)\, J_m(k_{m\mu} r_o)}{k_z [J_{m+1}(k_{m\mu} b)]^2} \tag{5}$$

$$* e^{i(k_z z - \omega t)}$$

from the form of equation 5, even though the dipole sound source distribution at z'=0 is selected to produce one particular θ-mode, all possible radial modes are also excited. However, each one is diminished by the $J_m(k_{m\mu} r_o)$ term appearing in equation 5. By using the tables from Jahnke and Emde [4] and the radial boundary condition $J_m'(k_{m\mu}) \Big|_{r=b} = 0$ to compute the $k_{m\mu}$'s, the

amplitude distribution of this term appears in Figures 3, 4, and 5 for the source ring radius as a percentage of the duct radius. Since only one θ-mode is developed at one time, depending upon the source distribution, each figure is thereby cross-plotted with the first few radial modes from 0 - 3.

As we have discussed previously, each (m,μ) mode becomes propagational at a different source frequency depending upon whether $k_z = [k^2-k_{m\mu}^2]^{1/2}$ is real or imaginary. The frequency at which a mode becomes propagational is known as its cutoff frequency. Each cutoff frequency for the radial modes appearing in figures 3,4, and 5 is listed to show,for example, for a 12"dia. duct the number of modes which can propagate depending on the source frequency selected. In general, however, what these curves indicate is that there is really no one optimum location for a source ring if one also desired control over the first few radial modes. Realistically though, one must choose a fixed source radius. The most efficient coupling to the duct apparently occurs between 10 to 20% and 90 to 100% of the duct radius. In our design we chose to locate our sources at 0.96 b. While this fixed radial position did not give us the greatest flexibility as compared to a variable ring radius, it does provide for the maximum number of (m,μ) modes to be generated efficiently. By using a variable source ring radius and the criterion for cutoff, one could conceivably selectively generate and propagate only one (m,μ) mode.

The results of this idealized analysis also indicates where not to locate the source ring. For the first few (m,μ) modes desired, care should be taken to avoid the zero crossings of the curves in figures 3,4, and 5 if one is to select a fixed source ring radius. Obviously, at these points an infinite source energy is required to propagate energy in the corresponding mode.

At this point then we must demonstrate that a discrete set of acoustic sources can generate one discrete θ-mode when coupled to a duct, realizing that the proper radial spacing of the sound sources is adequately determined as in Appendix C. Therefore equation 6 represents the (θ,t)

$$P(\theta t) = A_{mn} \cos(m\,\theta - nB\Omega t + \phi_{mn}) \qquad (6)$$

distribution of sound to be modeled from equation 1,and indicates that there will be for each harmonic of blade passage frequency an infinite number of left and right running lobed waves traversing in a helical path up the inlet duct. The waviness of the allowed lobed waves is determined by the index m. Figure 6 is a visualization of the concept of the spiral mode as it propagates down (or up) the duct and figure 7 represents for a fixed time the sound pressure distribution in the (r,θ) plane.

Since one of the major design features of the spinning mode synthesizer is the ability to generate one lobed structure at a time corresponding to a single blade passage frequency, equation 6 may be reduced to

$$P(\theta,t) = A_{mn} \sin(m\,\theta - nB\Omega t) \qquad (7)$$

where ϕ_{mn} is dropped because it represents only the phase relation among waves. Equation (7) corresponds to the acoustic pressure of one wave located in a plane normal to the duct axis. It is this relation which we wish to simulate by the spinning mode synthesizer.

ARRAY EQUATIONS

The preliminary objective in the development of the spinning mode synthesizer in this research was to demonstrate the feasibility of satisfying equation 7 in a free field test. Later developments were directed toward satisfying the conditions for a hard-walled duct. The easiest way to develop circumferential waves as defined in equation 7 would be to construct a device where sound sources are distributed circumferentially in a planar array as shown in figure 8. In order to satisfy equation 7, the drivers are sequentially phased around the circumference of the array. With the use of the coordinate system shown in figure 8, it can be shown that a system of n piston sources of equal strength (see Morse, 1968 [6]) radiates sound to the free far field as given by equation 8,

$$P(r,\theta,z,t) = A(k,D) \sum_{j=1}^{n} \frac{2J_1 (ka \sin \upsilon_j)}{ka \sin \upsilon_j} \frac{\sin(kR_j - \omega t + \phi_j)}{R_j} \tag{8}$$

where A(k,D) source sound pressure amplitude

a driver radius

k acoustic wave number of the driven piston

D driver separation

R_j, υ_j distance and solid angle respectively to radiation position from each source as defined in figure 8.

When υ is small, it is possible to choose a piston diameter of sufficient size to generate ample sound intensities but also so that $2J_1 (ka \sin \upsilon_j)/ka \sin \upsilon_j \sim 1$. Also in the far field small υ_j implies that R_j is practically constant. Therefore, besides the amplitude being a function of frequency and relative separation between sound sources, the sound pressure distribution in the far field is primarily sensitive to

$$\sum_{j=1}^{n} [\sin(kR_j + \phi_j - \omega t)] \tag{9}$$

The analogy with equation 7 becomes complete when we adjust ϕ_j such that

$$\sin(m\theta - nB\Omega t) = \sum_{j=1}^{n} [\sin kR_j + \frac{2\pi m}{n}(j-1) - \omega t] \qquad (10)$$

In other words, we should be able to generate spiral type waves when we provide phasing between drivers based on the simple relation

$$\phi_j = \frac{360m}{n}(j-1) \qquad (11)$$

when developing the (m,n)th wave.

In order to demonstrate that it was at least possible to develop the desired waveforms using the piston driver as a model, equations 8 and 11 were used to compute the free field sound pressure for various values of the parameters (m,f,ψ,n,D). In every case the desired waveform agreed identically with the expected distribution of sound pressure for the selected values of the above parameters. Later we will discuss the criterion for their selection, but numerically the circumferential mode index m was varied from 0 to 4, the driver frequency f from 1000 to 2500 Hz in 500 Hz increments, and the solid angle ψ from 10° to 20° in 5° increments. The number of drivers and their linear spacing D was fixed at 8 and 4.25" respectively.

Typical results of these calculations are shown in figures 9 through 18 for f = 2000 Hz only. As is immediately obvious from the curves of nondimensionalized sound pressure versus circumferential angle θ, the distribution of pressure is as expected for modal shapes 0 through 4. Perhaps though the decrease in SPL with a corresponding decrease in ψ is not as apparent. As will be demonstrated later, this occurs for all modes except m=0, since theoretically complete cancellation occurs at $\psi = 0$. This is a property of free-field operation only, for when coupled to a duct, the radial distribution is determined soley by the boundary conditions.

The time history at any two points, θ and $\theta + \delta\theta$, provide the opportunity for observation of the phase velocities of the generated waveforms. The curves in 14 through 18 for SP vs t clearly indicate each mode's direction of spin and angular velocity. For the jet engine compressor, the duct mode spin velocity is given by $nB\Omega/m$. For our proposed synthesizer, the modal spin velocity is given by ω/m as can be determined from these curves. If the base frequency is tuned to any multiple of the blade passage frequency so that $\omega = nB\Omega$, then our model's wave speed corresponds exactly to that of an actual engine for the same modal pattern. As is shown in the figures, the spin direction is determined by which of the two curves is leading or lagging the other in as much as the spatial point of measurement is known.

With regard to the feasibility of the spinning mode synthesizer, the proposed model performed satisfactorily. With appropriate phasing, high quality circumferential modes ranging from 0 to 4 can be generated under the idealized conditions as imposed by equation 8. Not only can the wave speed be controlled and determined, but also the wave's spin direction. Therefore, at least theoretically, the proposed model appears to be the flexible source of higher order duct modes for which we were originally in search.

THE EXPERIMENT

EXPERIMENTAL APPARATUS

In the last section, one sees that by using eight piston drivers without considering the effect of near field cancellation, one is able to generate the desired waveforms. In the design of the synthesizer, however, we had to provide for the most efficient arrangement of commercial loudspeakers which would minimize near field cancellation and at the same time behave as a piston type sound driver.

With regard to the acoustic efficiency of the array, Pritchard [7] presents curves of the normalized mutual radiation impedance for two piston drivers as a function of relative separation. This is his figure 2. By selecting D = 6", a = 1/2" and varying f from 1 to 3 kHz, Pritchard's data predicts that the mutual radiation impedance would be definitely within ± 0.2 for drivers in phase. While use of his data for drivers not in phase may be questioned, the curves still provide valuable guidelines to the design of a proposed system for minimizing near field cancellation.

With the spatial arrangement of the sound drivers determined by Pritchard's data, we found a rather inexpensive but extremely adequate loudspeaker with good frequency response and directionality characteristics similar to that of a piston driver. Figure 19 shows the selected loudspeaker and the agreement obtained between the two for loudspeaker frequencies of 1, 2, and 4 kHz. Since the device was to later be mounted to a duct, the solid angle ψ was limited to 0 to 20°. As can be seen for 2000 Hz , exact agreement is obtained between the piston driver and the selected loudspeaker directionality patterns for $\psi < 20°$. One, therefore, can expect reasonable operation of the proposed design in a duct for it satisfies the basic conditions of the analytical assumptions.

The experimental apparatus that was decided upon is shown schematically in figures 20 through 22. The overall assembly of figure 20 was mounted in Penn State's Anechoic Chamber for all subsequent free field tests. The sound driver array plate, figure 21, was installed in a 4 ft. diameter wooden baffle to simulate radiation to one side. The rear of the array was enclosed with a 2 ft. diameter fiberglass filled container. The purpose of this being to load each sound driver uniformly. Since each driver's output varied differently as a function of its input, it was found necessary to construct a probe tube microphone which could be rotated remotely to each sound driver. The output phase and sound pressure level of each driver could then easily be adjusted to desired values.

Two microphone processing systems were used for measuring the generated sound field in parallel and perpendicular planes from the driver array. The vertical plane of figure 8 was measured by the system shown in figure 22. As can be seen a 1/4" condenser microphone is mounted so that it could be rotated through 360° and indexed from 1" to 17" radially and up to 4' - 6' away from the sound driver array. The horizontal plane was processed by using a remotely controlled boom microphone system. A 1" condenser microphone was used to record the directivity patterns of the entire array from radii of 2.5 to 4 feet.

EXPERIMENTAL PROCEDURE

The purpose of the experiment was, of course, to verify that one could selectively generate higher order θ duct modes with the proposed design. In order to demonstrate this, measurements in planes parallel to the driver array were carried out according to the following schedule. Since very little difference exists between the radiated sound patterns for the ducted and unducted driver array when the solid angle ψ is less than 20° (See figure 8), all of the following preliminary testing was conducted with the array mounted under free field conditions. The 1/4" microphone was positioned at 2.5, 3.0, 3.5, and 4.0 ft. away from the driver plane and rotated 360° for microphone radii from 1" to 17" which corresponded to the solid angles of 5°, 10°, 15°, and 20° at each respective location. This was done for modes 0 through 3 and for driver frequencies of 1500, 2000, and 2500 Hz . Figures 23 and 24 characterize the electronic drive system used to supply each of the eight drivers in the array and also the electronics used in processing the data from the 1/4" and 1" microphones.

EXPERIMENTAL RESULTS AND DISCUSSION

We will first present data for the array's directivity. In figures 25 through 28 solid lines show the recorded directivity of the entire array for a driver frequency of 2000 Hz only for modes 0 through 3. The only observed change when the driver frequency increased was a decrease in overall beam width for all patterns. The dashed curves are generated from Tyler and Sofrin's equation 7.3.2 which describes radiation from a circular duct with the additional possibility of radial modes. It is particularly interesting to note the remarkable agreement between the array's directivity and that predicted by 7.3.2. The agreement appears best with the radial mode $\mu = 1$. This corresponds to physical reality, since if we recall figure 26 from Tyler and Sofrin, we observe that if we phase our drivers for m =1, the mechanical location of the drivers dictates approximately a near field pressure distribution of $\mu = 1$ as shown in the figure. It is not surprising then that with a single ring of drivers the near field pressure pattern as arranged in our design would always simulate a (m,1) mode of an open face circular duct.

Because of the very good agreement exhibited in figures 25 to 28, one should be able by using various number of driver rings to simulate accurately any (m,μ) mode radiated from a fan or compressor inlet duct. The utility in doing this may be realized if one seeks to determine the original near field pressure pattern of a frequency spectrum from the noise field of a full scale engine. Such a spectrum appears in figure 26 from directivity measurements carried out by Morfey and Dawson [8] on a full scale turbojet engine. The data used corresponds to their engine B and the directivity measurements of figure 2a where in our case the $S/s\lambda$ parameter equals 0.393. Agreement appears good up to 45° off axis, where beyond this the turbojet's broadband spectrum becomes dominant.

Perhaps more convincing results are presented in figures 29 through 35. These curves represent the measured RMS sound pressure in a plan parallel but 4' distant from the sound driver array. For the sake of brevity, only the data taken at this distance for modes 0 through 3 at a driver frequency of 2000 Hz are presented. There are actually two sets of curves. Figures 25 through 28 delineate the measured phase angle between positions in the plane for microphone radii of 7.625", 12.345", and 17.275". The second set of curves, figures 29 to 35, represent for any arbitrary fixed time the resulting spatial waveform.

An obvious bounding condition upon the operation of the synthesizer rests with its ability to generate the plane wave. Figure 29 shows that it is possible to generate the plane wave to within $\pm 5°$ of phase at the indicated measurement position. In these curves phase is measured with respect to the $\theta = 0°$ position as shown in figure 8. Perhaps the deviation in this curve can be better understood by reference to figure 25. There, the array's directivity for m = 0 indicates that the main beam has a slight asymmetry. Since this measurement was carried out with the 1/4" rotating microphone drive disassembled, reflection from that processing system can probably be ruled out. During these tests each driver's output was sensed to be within $\pm 0.5°$ of phase and driven at the same output level. But these numbers were only accepted from the center of each speaker's output. Sufficient care was not taken at this time to measure accurately the entire near field pressure level and phase existing over the entire near field area of each driver. Variations in driver characteristics are believed to produce the deviation shown in figure 11a. Later experiments with better model drivers verified this hypothesis. Since all measurements at different axial locations and solid angles exhibit the same basic deviation from the expected wave, it is felt at this time that nonuniformities of each driver's near field sound distribution is the principal basis for the majority of the discrepancy. In future experiments one would be wise in the purchase of commercial sound drivers of higher quality.

As can be seen in figures 30, very good agreement between measured and expected phase distribution is obtained when phasing for mode 1. Apparently, as the solid angle ψ was increased from 15° to 25° a greater divergence from the expected distribution occurs. With reference to the array's directivity for mode 1, figure 26, one can infer that the effect of driver inhomogeneities on the mutual impedance between drivers manifests itself in producing a more distorted near pressure field. This trend continues as the phase angle is increased between drivers to generate modes 2 and 3 as is evidenced by figures 31 and 32 resprectively.

It is possible to calculate the mode shapes from the first set of curves and measurements of the sound pressure level at each of the θ-coordinate positions where phase was recorded. This essentially results in the sound pressure distribution as a function of θ for an arbitrary fixed time. Once again the $\theta = 0°$ position was chosen to correspond to maximum amplitude for the time selected and the other points were calculated from this reference. In each curve of figure 33 to 35 the expected waveform is plotted on the basis of the average amplitude which was recorded from all the measurements.

For mode 0 excellent agreement is obtained with the expected distribution, and as is evidenced in figure 34 the waveforms for modes 1 and 2 demonstrate that it is very possible to generate with the synthesizer high quality spinning waves. As may be expected from viewing figure 28, the near field interaction between sound drivers induces considerable far field distorted signals when phasing for mode 3. In fact one should not expect a reasonably defined waveform for solid angles $\psi < 20°$. Since this constitutes the maximum solid angle for measurements, data for mode 3 is not presented. In any case the results appear satisfactory, in the sense that at least up to mode 2 high quality spinning waves can be generated using only eight equally spaced drivers in a single ring.

CONCLUSIONS

This report describes research directed toward the development of a device capable of simulating the discrete set of eigenfunctions as produced by fan or compressor vehicles. The system we chose consisted of only eight piston-like sound drivers which permitted only the development of the first two spinning modes. Figures 34 and 35 clearly indicate that for this system the modes which were developed were of high quality, and the ease by which $nB\Omega$ and m could be changed provides an excellent means for parameter variation when this system is coupled to a duct to study the attenuation properties of various acoustic materials in the presence of these spinning waves.

When coupling this device to a duct, it has been determined as in Appendix C that the most efficient location for the sound drivers would be in the outer 10% of the duct radius. In this position the maximum number of (m,μ) modes could be selectively generated and propagated in the duct.

Finally, the results of figure 26 suggest that this device could also be used to study the sound pressure distribution of an engine inlet by synthesises of its sound field. Since reliable sound measurements are difficult in the presence of airflow at the engine inlet, the far field directivity patterns of the engine and synthesizer could be measured and compared, and the latter adjusted to give identical results on a filtered peak.

APPENDIX A

Symbols

a	piston or driver radius
A_{mn}	amplitude of the (m,n)th mode
b	duct radius
B	# of rotor blades
c	local sound speed
c_r	radial phase velocity
c_z	axial phase velocity
c_θ	circumferential phase velocity
d	hub radius
D	sound driver separation
$E^{\sigma}_{m\mu}$	radial duct eigenfunction
k	acoustic wavenumber
$k^{\sigma}_{m\mu}$	radial duct eigenvalue
k_z	axial duct eigenvalue
m	circumferential duct eigenvalue
n	harmonic of blade passage frequency (time eigenvalue)
P	acoustic sound pressure
Q	source acoustic volume flow rate
r	radial coordinate
r_o	source ring radius
R_j	distance from driver plane (defined in figure 8)
u_ω	source volume velocity
V	# of stator vanes
z	axial coordinate

α	spiral angle in the (r,θ) plane
$\delta(\underline{x}-\underline{x}')$	the Dirac delta function
ε_m	1 when $m = 0$, and 1/2 when $m > 0$
θ	circumferential coordinate
μ	radial mode index
ρ	fluid density
σ	hub tip ratio (d/b)
υ_j	solid angle from origin of each driver (defined in figure 8)
ϕ_j	adjustable phase of each sound driver (equation 11)
ϕ_{mn}	phase of (m,n)th mode
ψ	solid angle from the origin of driver plane (defined in figure 8)
ω	radian frequency of compressor or sound drivers
Ω	rotor RPM

APPENDIX B

Calculation of the Allowed Order of Circumferential Modes

The derivation for the allowed order of circumferential modes does not appear in any way to be unique. The procedure adopted here relies mainly upon a suggestion proposed by Bragg and Bridge [2] which treats the geometrical characteristics of propagating spiral waves from a ducted rotor-stator interaction. In figure B1 we attempt to show how the periodic redistribution of pressure over rotor blades due to the stator velocity defect gives rise to a fluctuating lift force. Now it is known (See Lowson[3]) that fluctuating lift forces gives rise to dipole sound fields and a careful observation of the coordinates of the wake-blade interaction zone reveals that there are v(# of stator vanes) interaction zones fixed at regular intervals of $2\pi/v$ radians in the θ coordinate. In each zone the dipole pressure pulse moves from the hub to the tip of the rotor in a cyclic fashion with a period of $2\pi/v\Omega$ seconds.

As discussed in the main text, those normal modes, (m,μ) for which equation 2 is real are propagated unattenuated in the duct. As is obvious, should a propagating mode be one with $m > 0$, then its wavevector or direction of propagation will be directed off-axis. Thus its lines of constant phase which define the wavefront will form a helical curve of increasing pitch diameter along the duct axis. This condition is shown schematically in figure 6 and its distribution for a fixed time in figure 7.

The spiral angle of these wavefronts formed in the (θ,z) plane is determined by the vector addition between circumferential and axial particle phase velocities as is expressed by equation B1. Since all acoustic disturbances

$$\frac{1}{c} = \frac{1}{c_r} + \frac{1}{c_\theta} + \frac{1}{c_z} = \frac{1}{c_r} + \frac{1}{cx}$$

$$c_x = \frac{c_\theta c_z}{c_z + c_\theta} \qquad \text{(B1)}$$

propagate at the local sound speed, their circumferential phase velocity must be sufficiently supersonic to guarantee a sonic condition at the wavefront. Otherwise the velocity triangle in figure B2 could never be satisfied. As one can see, the circumferential phase velocity is proportional to the rotor speed Ω, number of rotor blades B, harmonic index n, and radius r, but inversely proportional to the circumferential mode number m.

As is indicated in figure B1, the spiral angle α is given by

$$\sin\alpha = \frac{cx}{c_\theta} = \frac{cx\ m}{2\pi nB\Omega r} \qquad \text{(B2)}$$

As we have mentioned previously, we can consider the interaction of a rotor and stator wake to consist of v sources of pulsating pressure. By definition, the acoustic pressure radiated from each of these sources will arrive in phase along all points which define the wavefront. Shown in figure B3 is a row of stator sources radiating sound in such a manner that the wavefront forms the spiral angle α in the $(\theta\text{-}z)$ plane. At the point P, the acoustic pressure is in phase with each source by any multiple of 2π. This, of course, implies that the phase relation among the sources coupled with varying distances between P and each source must add to be a multiple of 2π. For a rotor cascade consisting of B blades and rotating at Ω rad/sec, this can be expressed as follows:

Source Phase Rotation		Phase from Increased Distance
$\frac{2\pi}{V\Omega} * nB\Omega$	+	$\frac{2\pi \sin \alpha}{c_x V} * nB\Omega r = 2\pi h$

where $h = 0, \pm 1, \pm 2, \ldots$ Equations B2 and B3 can be solved simultaneously for m producing the classical result first reported by Tyler and Sofrin [1] and given by equation B.3.

$$m = nB + hV \tag{B.3}$$

APPENDIX C

Effect of Source Location on Output Spectrum

Consider the radiation of sound from a ring of simple sources with a specified θ distribution into a semi-infinite rigid tube closed at $z = 0$. This configuration is displayed in figure 2. Assuming that the sound field is simple harmonic, $P(x,t) = P_\omega(\underline{x})\, e^{-i\omega t}$, then the classical homogenous Helmholtz equation to be solved is

$$\nabla^2 P_\omega(\underline{x}) + k^2 P_\omega(\underline{x}) = 0 \tag{C1}$$

with the inhomogenous boundary condition at $z = 0$, i.e.

$$\left.\frac{\partial P_\omega}{\partial z}\right|_{z=0} = i k \rho c u_\omega(r',\theta') \tag{C2}$$

where the volume velocity is specified to be Q for the particular case of all sources in phase and is given as

$$\mu_\omega(r',\theta') = \frac{Q}{2\pi r'} \cos(n\theta' + \phi_n')\, \delta(r-r_o) \tag{C3}$$

The remaining boundary conditions are those typically expected for a circular rigid tube with no reflected waves, and are

1) $\partial P_\omega/\partial r = 0$ at $r = b$ and $\partial P_\omega/\partial z = 0$ at $z = 0, \neq z'$

2) P_ω is finite as $r \to 0$ and $z \to \infty$

3) P_ω and $\partial P_\omega/\partial\theta$ continuous at $\theta = 0, 2\pi$

In general, the most useful technique for solving the above system is to make use of the appropriate Green's function associated with the eigenfunctions of the completely homogenous system. Essentially this offers the greatest flexibility should one later decide to refine the acoustic source function into a more realistic distribution. The most efficient method for determining the Green's function for this problem is by the method of eigenfunction expansion. This technique is described particularly well by Morse and Feshbach [5] and is valid since the system is entirely self-adjoint. Applying this technique, we find that the appropriate Green's function for this problem which satisfied the adjoint boundary conditions, continuity at the source plane, and the jump condition in the first derivative is given by

$$G_\omega(\underline{x},\underline{x}') = -\frac{i\varepsilon_m}{\pi b^2} \sum_{m,\mu} \frac{\cos(m\theta+\phi_m)\cos(m\theta'+\phi_m')\, J_m(k_{m\mu}r)\, J_m(k_{m\mu}r')}{k_z\,[J_{m+1}(k_{m\mu}b)]^2} \tag{C4}$$

$$* \begin{cases} \cos k_z z\; e^{ik_z z'} & 0 \le z < z' \\ \cos k_z z'\; e^{ik_z z} & z > z' \end{cases}$$

where $\varepsilon_m = \begin{cases} 1 & m = 0 \\ 2\left(\dfrac{k_{m\mu}^2 b^2}{m^2} - 1\right) & m > 0 \end{cases}$

$$k_z = \left[\left(\frac{\omega}{c}\right)^2 - k_{m\mu}^2\right]^{1/2}$$

$k_{m\mu}$ = set of numbers generated by $\left.\dfrac{\partial J_m(k_{m\mu} r)}{\partial r}\right|_{r=b} = 0$

When observation of the tube sound pressure is desired for positive axial displacements away from the source plane the lower z-coordinate eigenfunction appearing in braces in C.4 is to be used.

At this point we can make use of Green's cookbook formula for determining the tube's sound pressure field, i.e.

$$P_\omega(\underline{x}) = \iiint s_\omega(\underline{x}') \, G_\omega(\underline{x},\underline{x}') \, d V'$$

$$+ \iint \left\{G_\omega(\underline{x},\underline{x}') \frac{\partial P_\omega(\underline{x}')}{\partial z} - P_\omega(\underline{x}') \frac{\partial G_\omega(\underline{x},\underline{x}')}{\partial z'}\right. d S'$$

Since there are no sources inside the tube's volume and the outward pointing normal gradient of the Green's function is zero, we only need to evaluate the surface integral as given in equation C.5. Inserting

$$P_\omega(\underline{x}) = \iint G_\omega(\underline{x},\underline{x}') \frac{\partial P_\omega(\underline{x}')}{\partial z'} \, r' \, dr' \, d\theta' \qquad \text{(C5)}$$

equations C.2, C.3, and C.4 into C.5 the tube's sound pressure field is found to be with the source plane at $z' = 0$

$$P(\underline{x},t) = P_\omega(\underline{x}) \, e^{-i\omega t}$$

$$= \frac{\varepsilon_m k \rho c Q}{(2\pi)(\pi b^2)} \sum_{m,\mu} \frac{\cos(m\theta+\phi_m) \, J_m(k_{m\mu} r) \, J_m(k_{m\mu} r_o)}{k_z \left[J_{m+1}(k_{m\mu} b)\right]^2}$$

$$* \int_o^{2\pi} \cos(m\theta'+\phi_m') \cos(n\theta'+\phi_n') \, d\theta'$$

This last integral is identically zero unless $m = n$, which implies that the only θ-tube mode excited corresponds exactly to the desired θ source distribution. When $m = n$ the value of the integral is π and we have finally for the tube sound pressure

$$P(\underline{x},t) = \frac{\varepsilon_m \, k \rho c Q}{2\pi b^2} \frac{\cos(m\theta+\phi_m) \, J_m(k_{m\mu} r) \, J_m(k_{m\mu} r_o)}{k_z \left[J_{m+1}(k_{m\mu} b)\right]^2} \qquad \text{(C6)}$$

$$* \, e^{i(k_z z - \omega t)}$$

References:

1. Tyler, J. M. and Sofrin, T. G.: Axial Flow Compressor Studies, SAE Trans. pp 309-332, 1961

2. Bragg, S. L. and Bridge, R. : Noise From Turbojet Compressors, J. of the Royal Aeronautical Society, 66: 1-10, 1964

3. Lowson, M. V. : Reduction of Compressor Noise Radiation, J. of the Acoustical Society of America, 43: 37-50, 1968

4. Jahnke, E. and Emde, F. : Tables of Functions, Dover 1945, 4th Edition

5. Morse, P. M. and Feshbach, H. : Methods of Theoretical Physics, McGraw Hill, 1953, Vol. 1, page 820

6. Morse, P. M.: Vibration and Sound, McGraw Hill Book Company, Inc. New York

7. Pritchard, R. L. : Mutual Acoustic Impedance between Radiators in an Infinite Rigid Plane, J. A. S. A., Vol. 32

8. Morfey, C. L. and Dawson, H. : Axial Compressor Noise, A. S. M. E., 11th Annual Gas Turbine Conference, Zurich, 1966

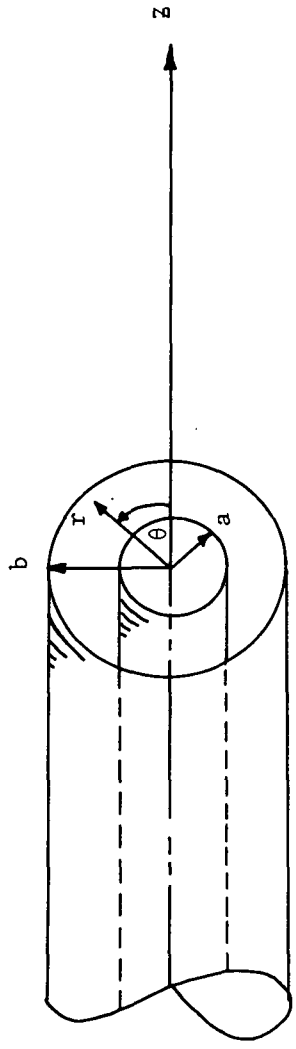

Figure 1 Duct Coordinate System

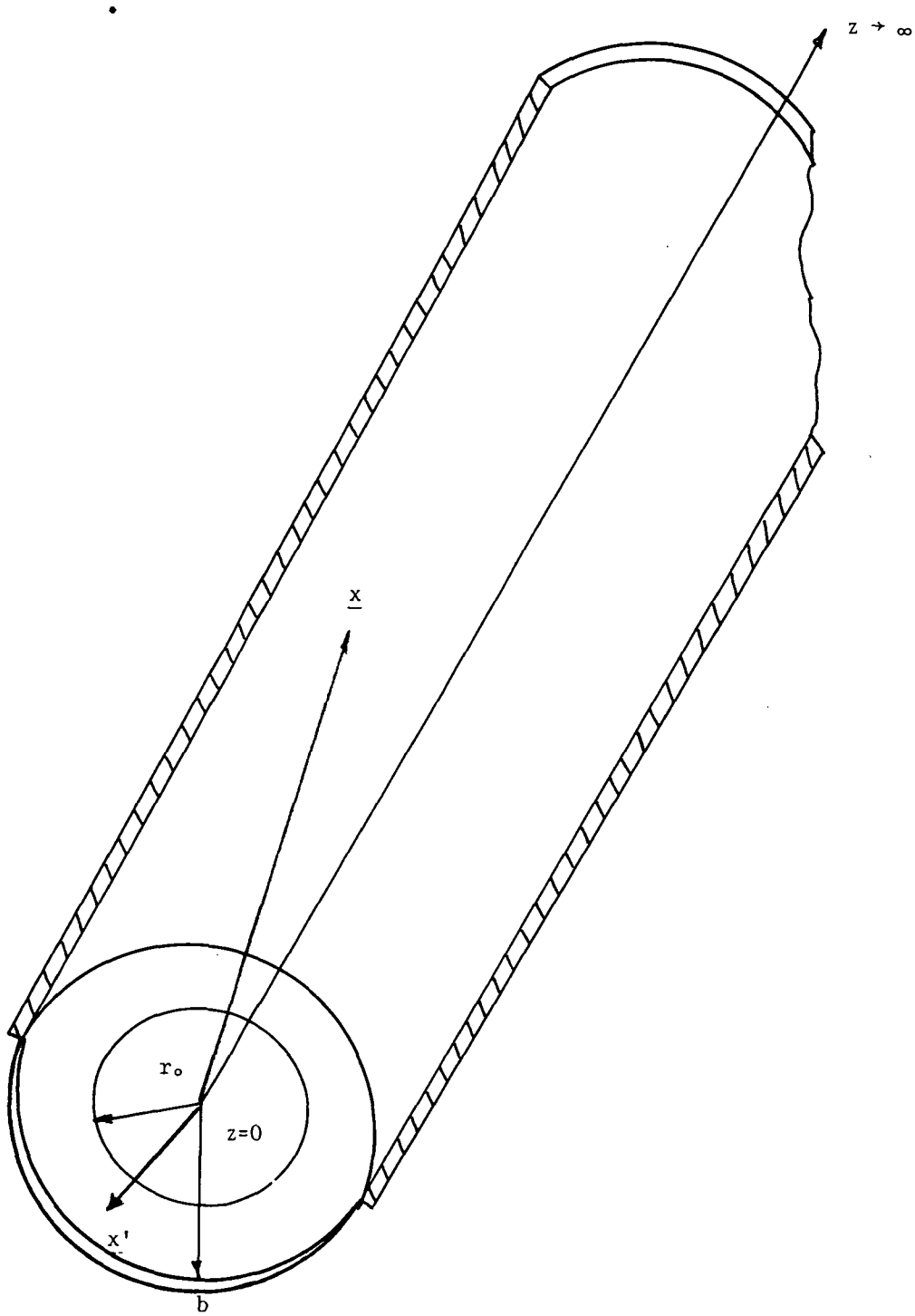

Figure 2 Source Ring Coordinate System

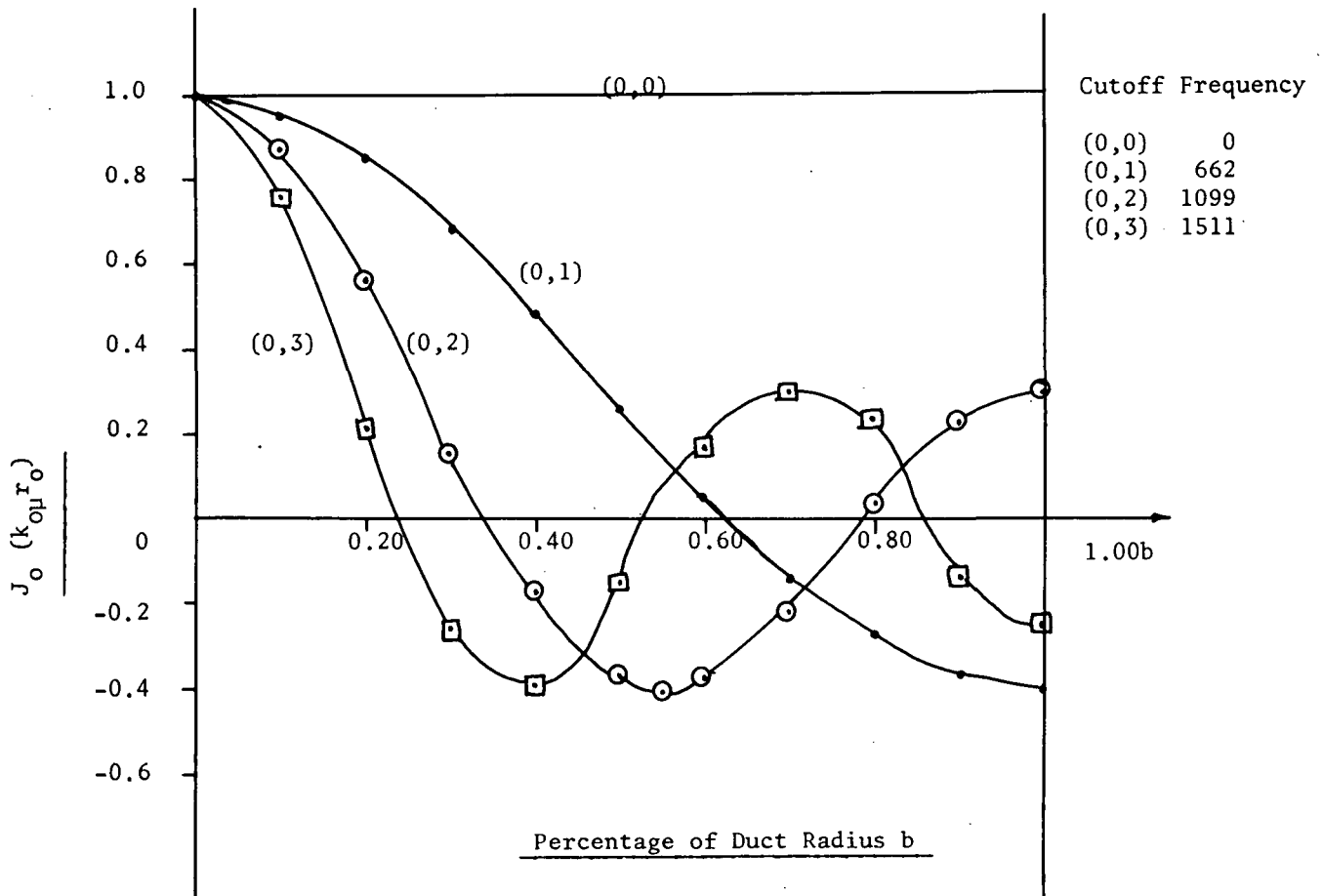

Figure 3 Attenuation Factor $J_o (k_{o\mu} r_o)$

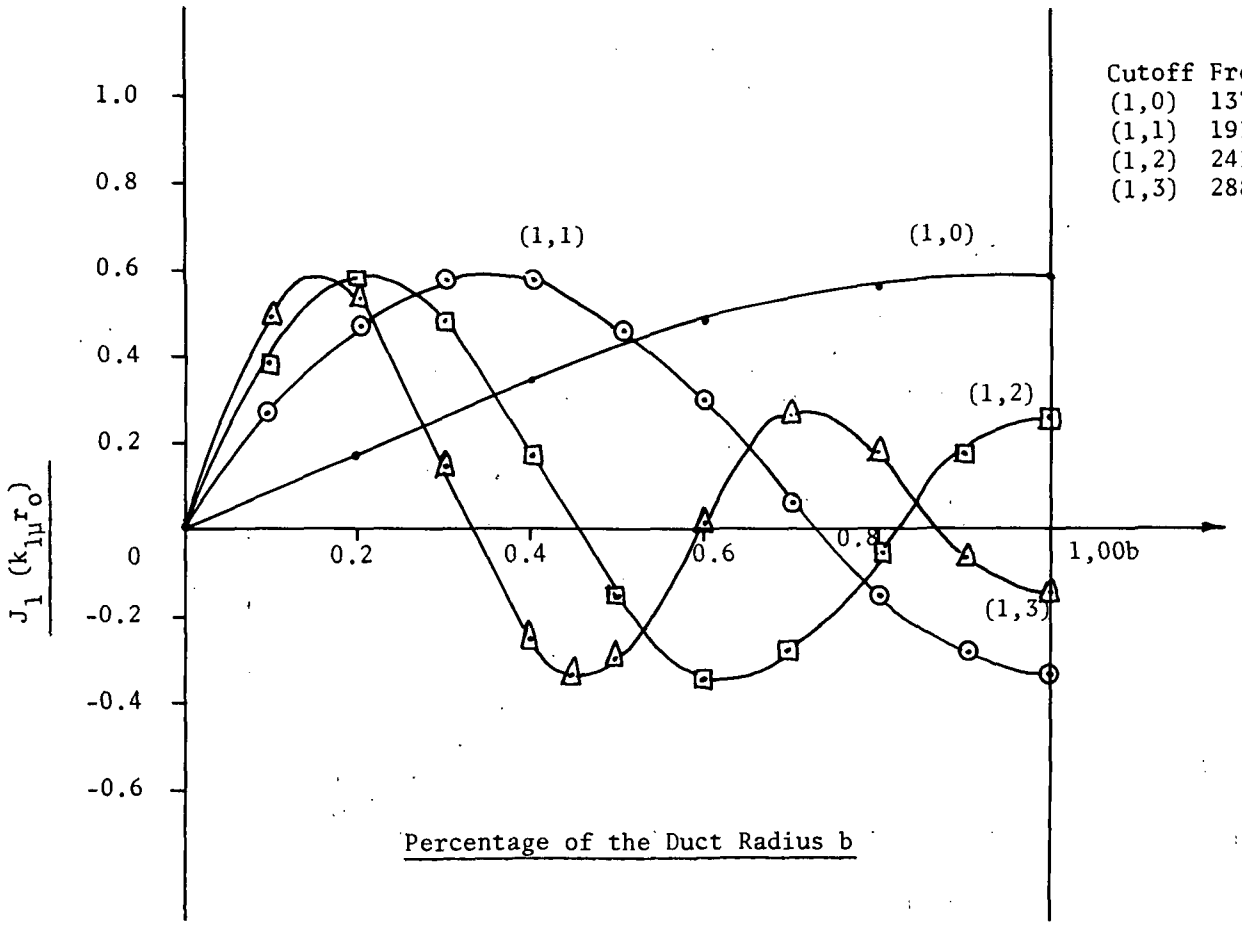

Figure 4 Attenuation Factor $J_1 (k_{1\mu} r_o)$

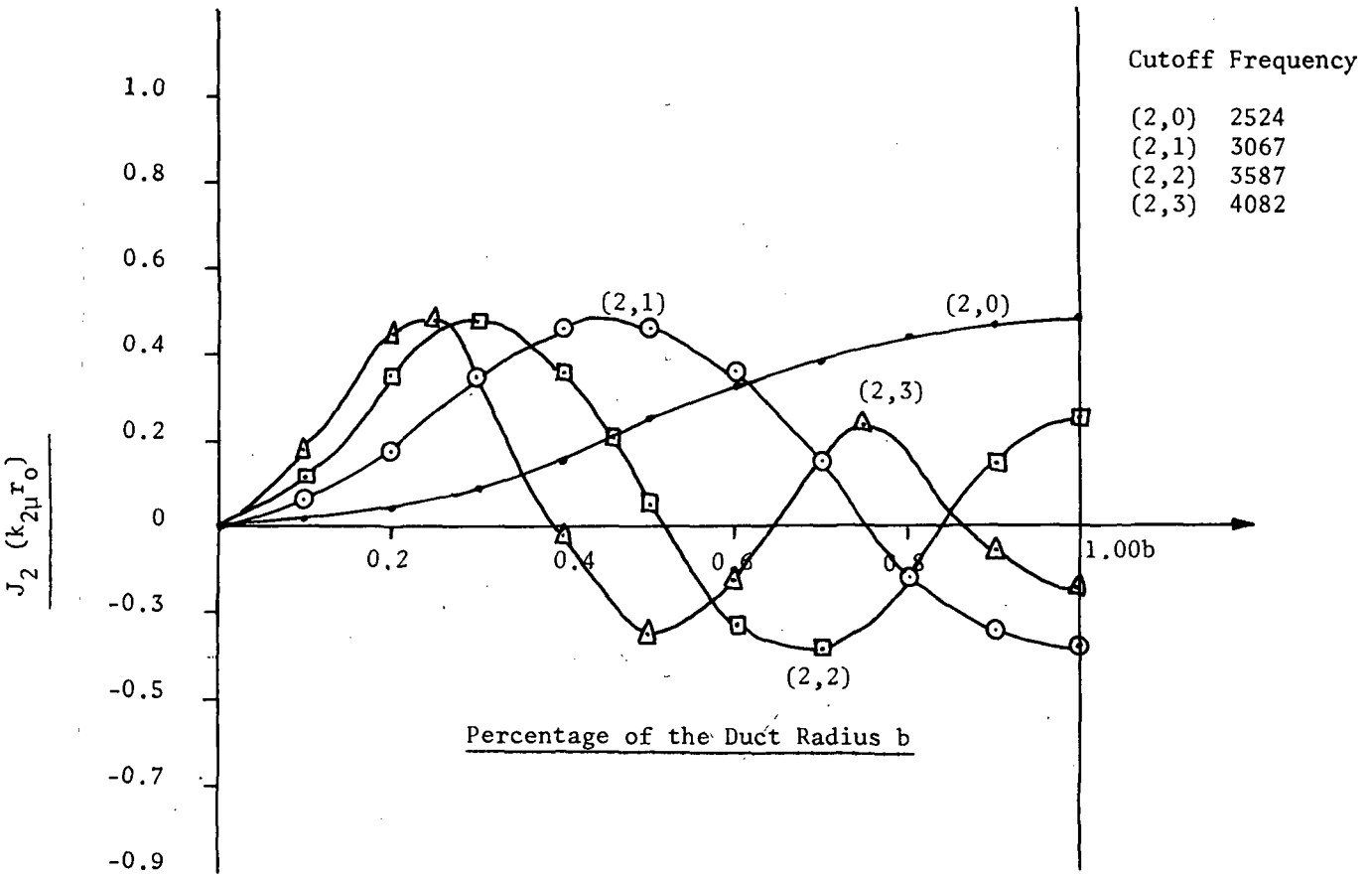

Figure 5 Attenuation Factor $J_2 (k_{2\mu} r_o)$

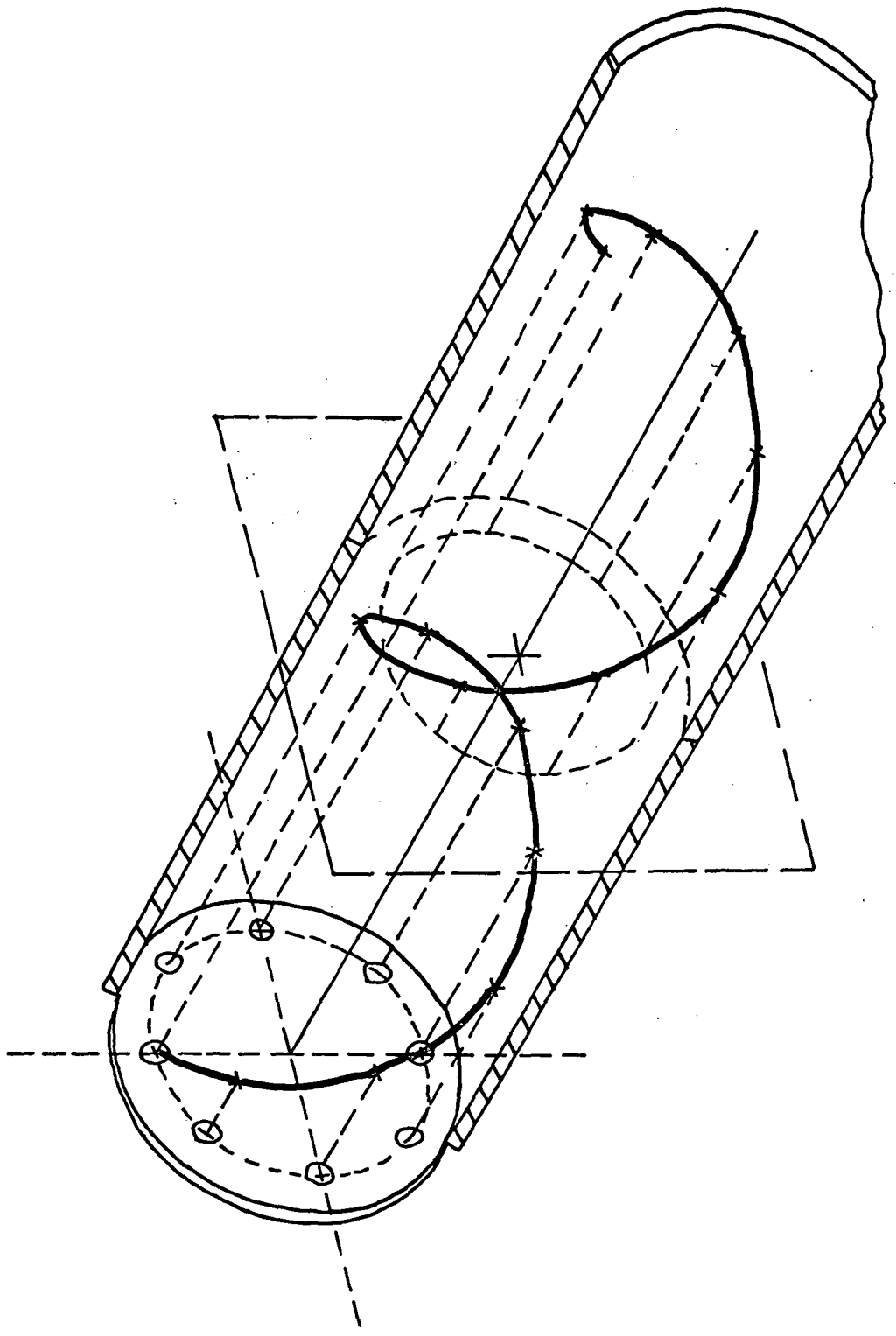

Figure 6 Visualization of Spiral Wave

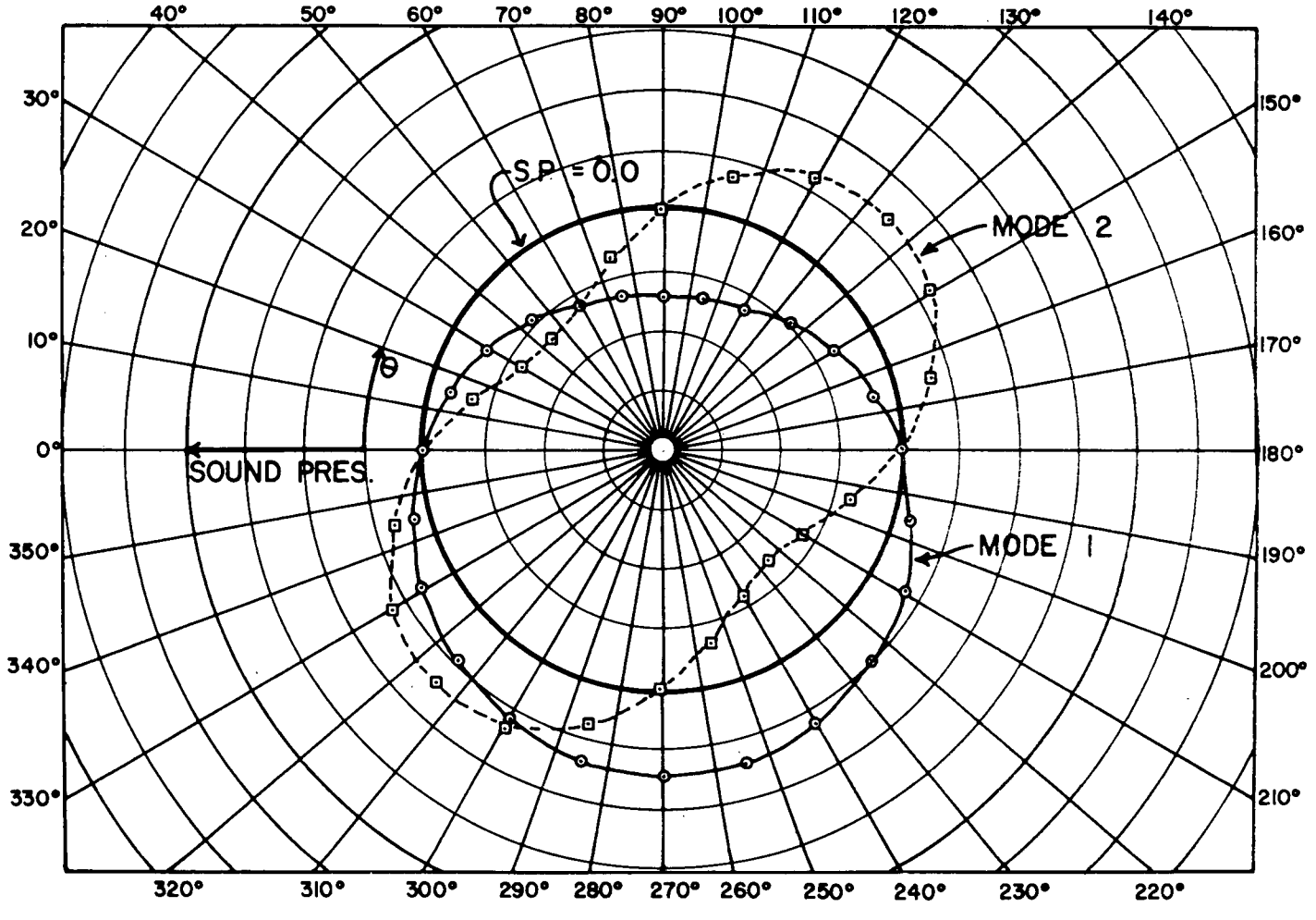

Figure 7 Predicted Waveforms in the (θ,r) Plane for a Fixed Time

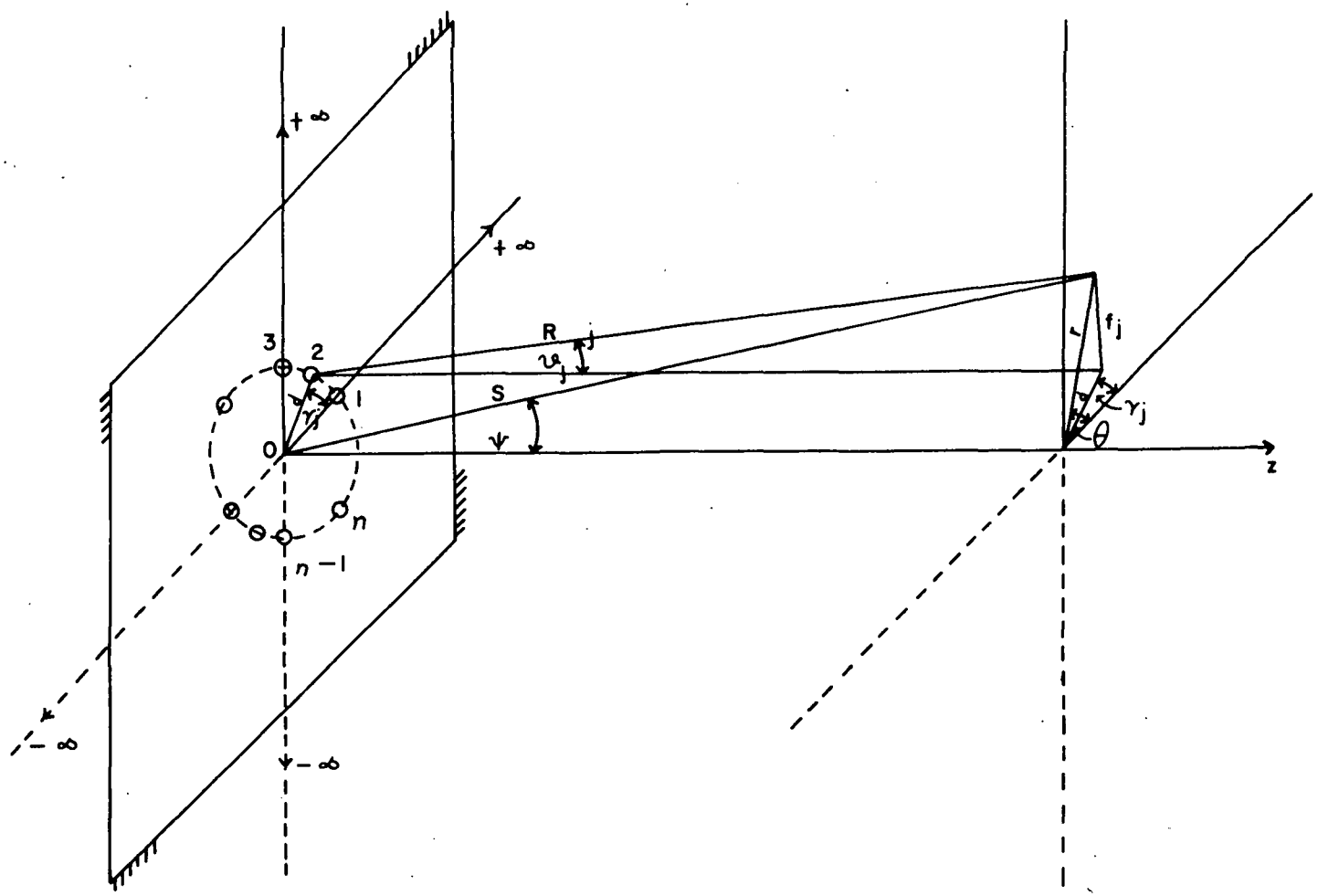

Figure 8 Coordinate System for Determining Acoustic Field of a System of n Sound Drivers

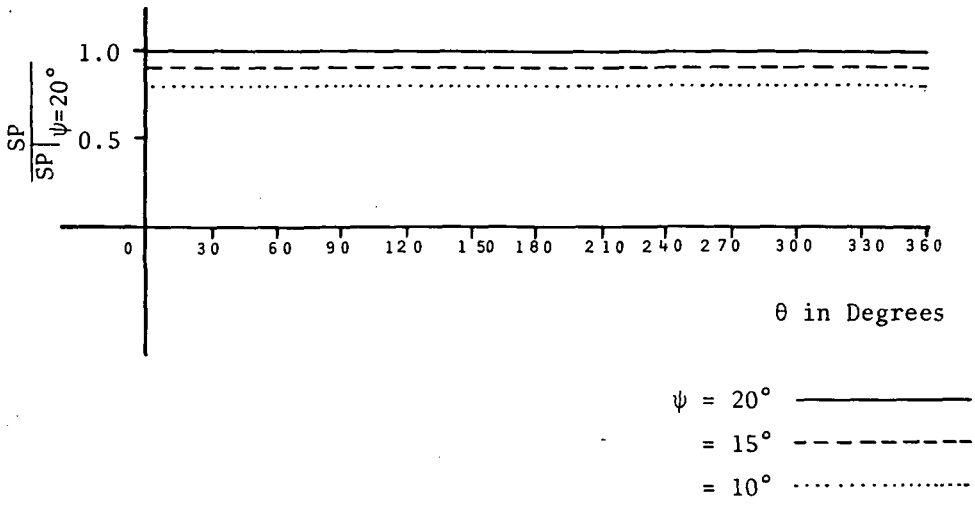

Figure 9 Calculated Sound Pressure Level vs. Theta for Mode 0 at 2000 c/s

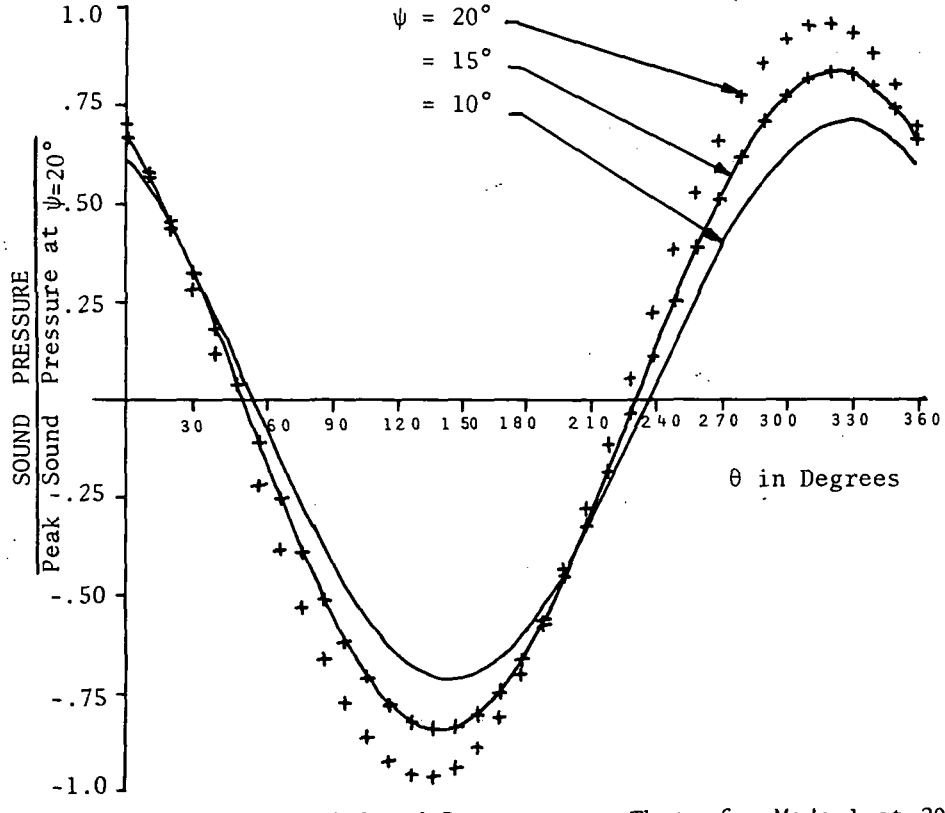

Figure 10 Calculated Sound Pressure vs. Theta for Mode 1 at 2000 c/s.

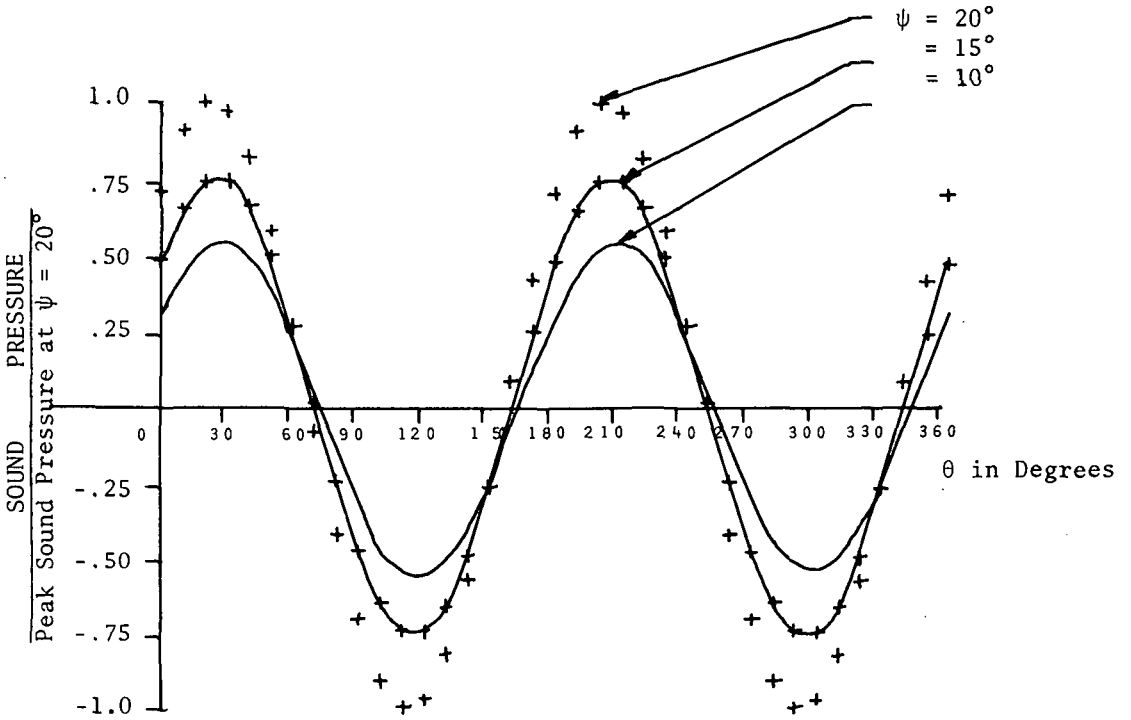

Figure 11 Calculated Sound Pressure vs. Theta for Mode 2 at 2000 c/s.

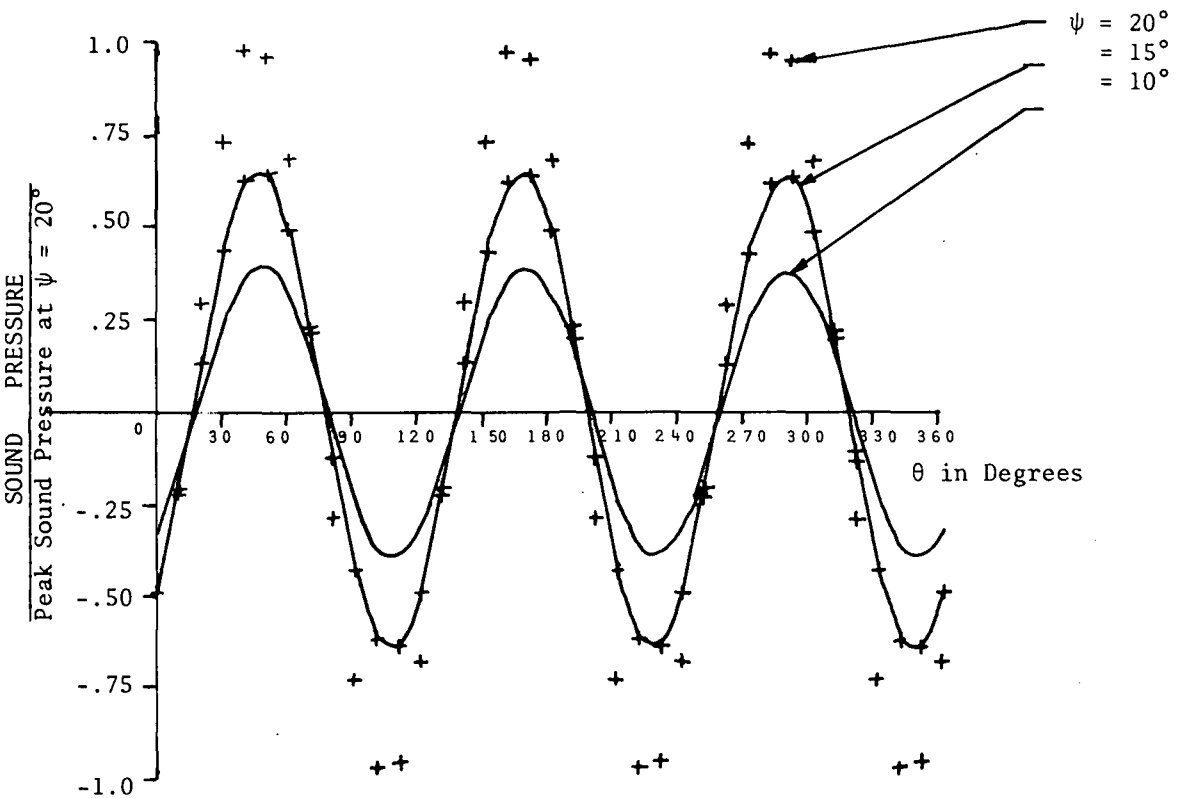

Figure 12 Calculated Sound Pressure vs. Theta for Mode 3 at 2000 c/s.

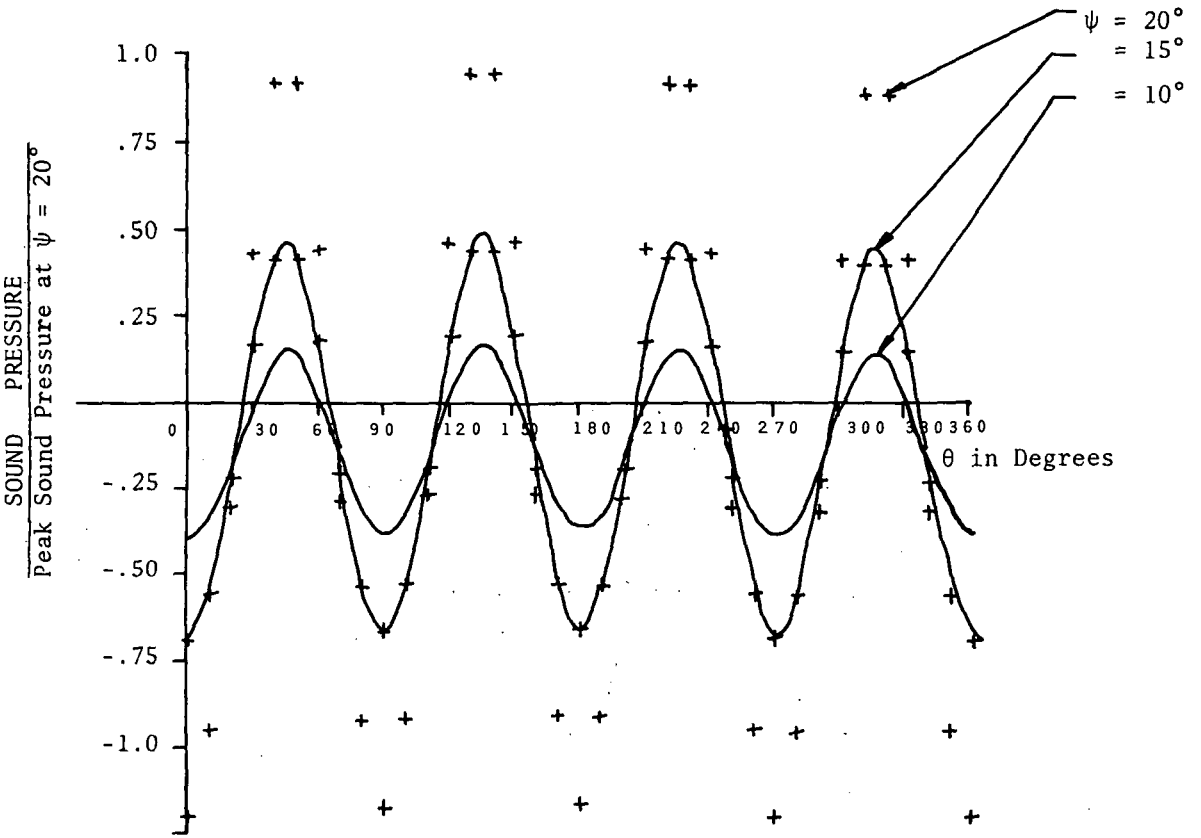

Figure 13 Calculated Sound Pressure vs. Theta for Mode 4 at 2000 c/s.

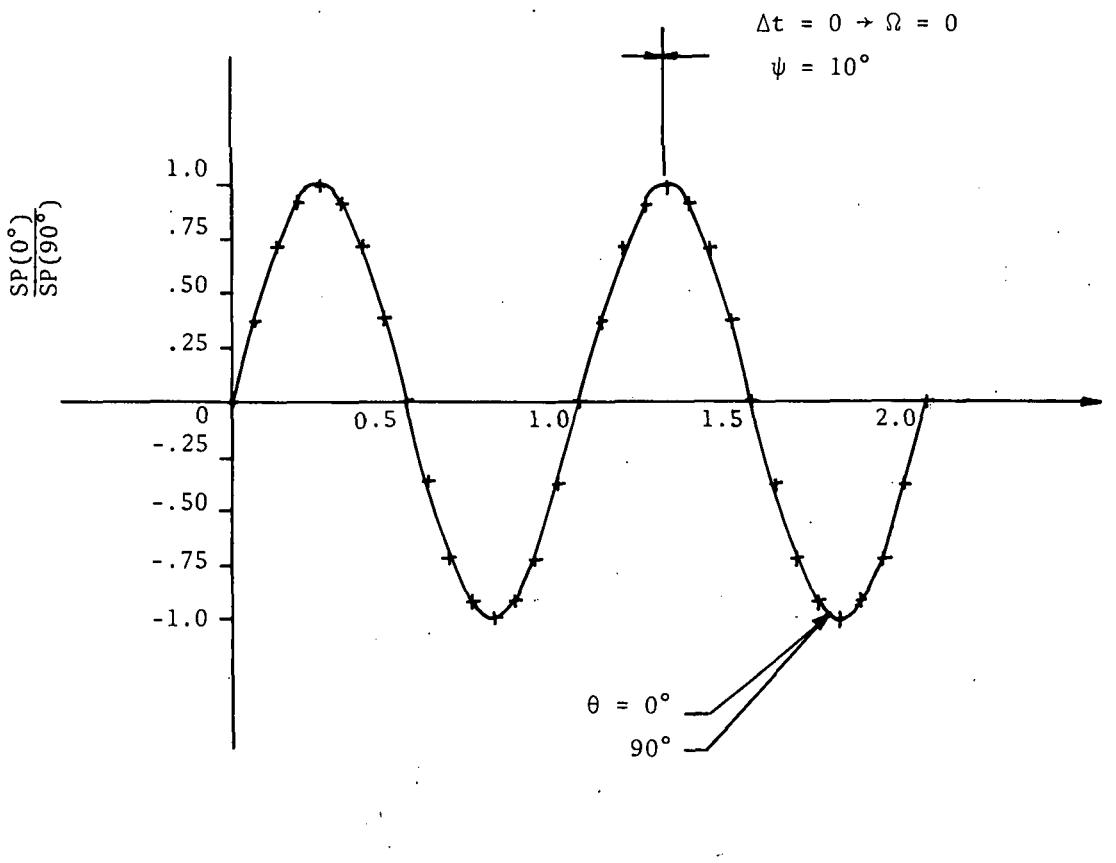

Figure 14 Calculated Sound Pressure vs. Time for Mode 0 at 2000 c/s

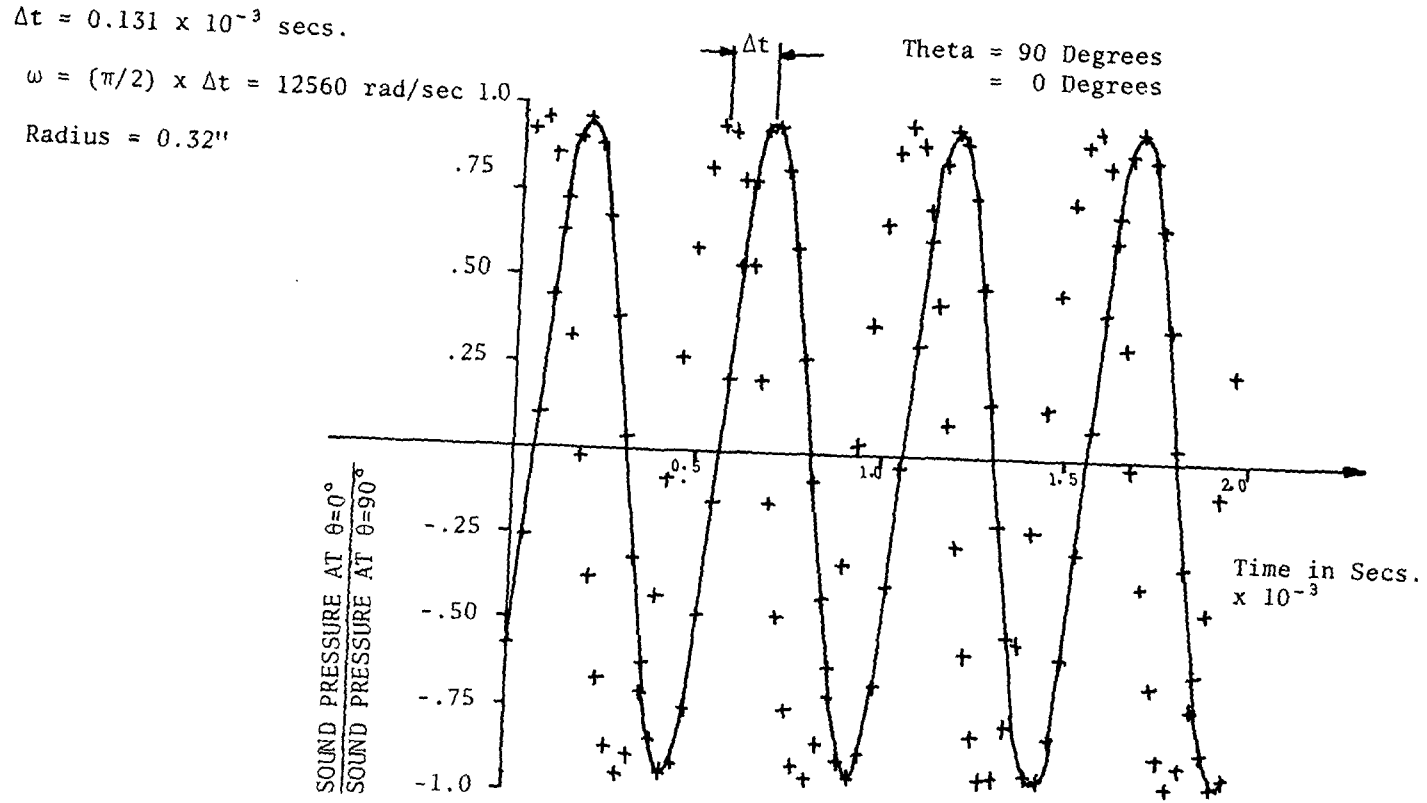

Figure 15 Calculated Sound Pressure vs. Time for Mode 1 at 2000 c/s.

$\Delta t = 0.262 \times 10^{-3}$

$\omega = (\pi/2) \times \Delta t = 6280$ rad/sec.

Radius = 6.32"

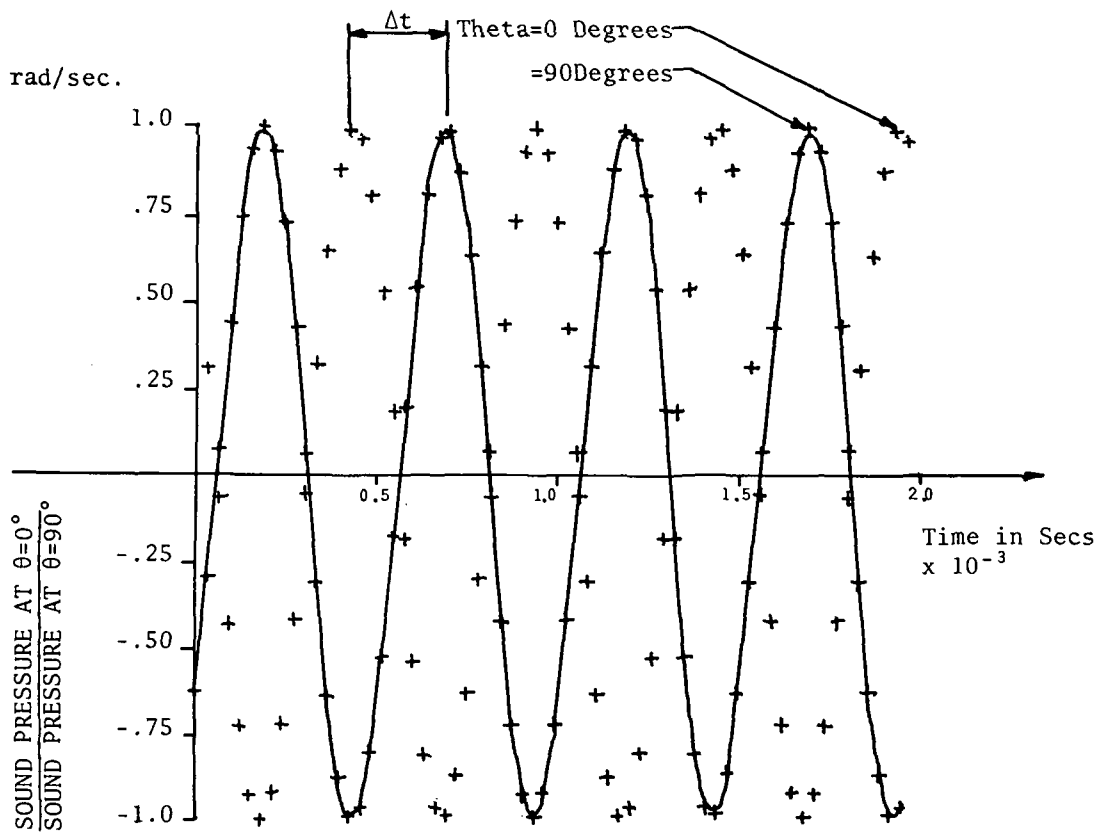

Figure 16 Calculated Sound Pressure vs. Time for Mode 2 at 2000 c/s.

$\Delta t = 0.393 \times 10^{-3}$ secs.

$\omega = (\pi/2) \times \Delta t = 4187$ rad/sec.

Radius = 6.32"

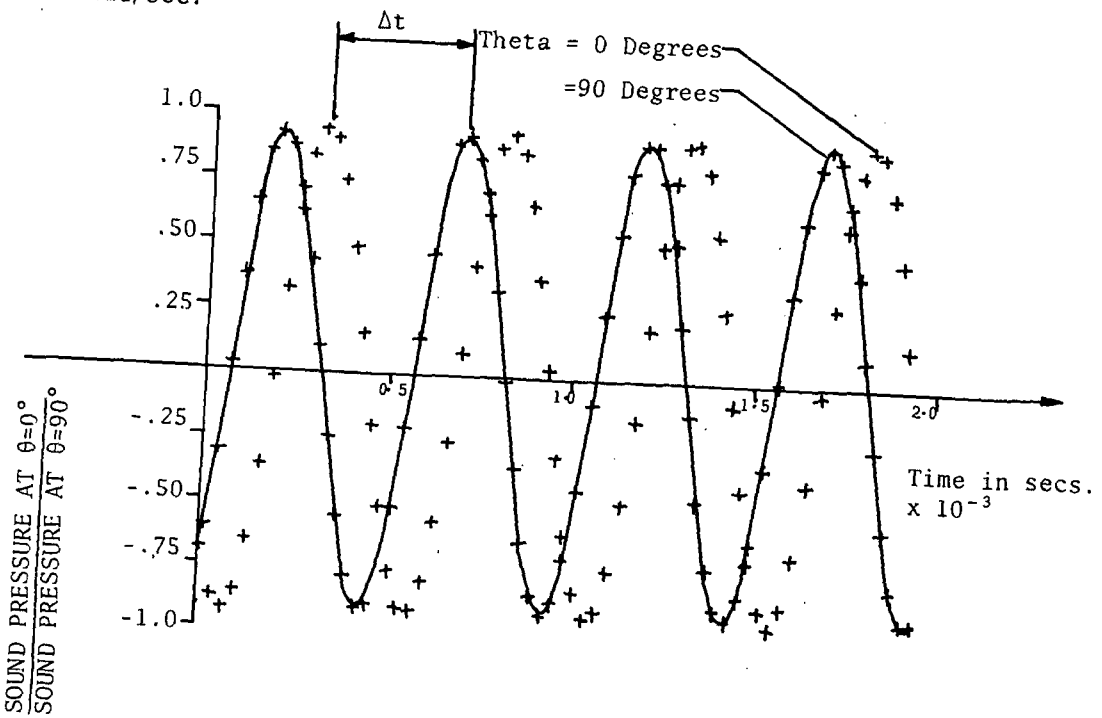

Figure 17 Calculated Sound Pressure vs. Time for Mode 3 at 2000 c/s.

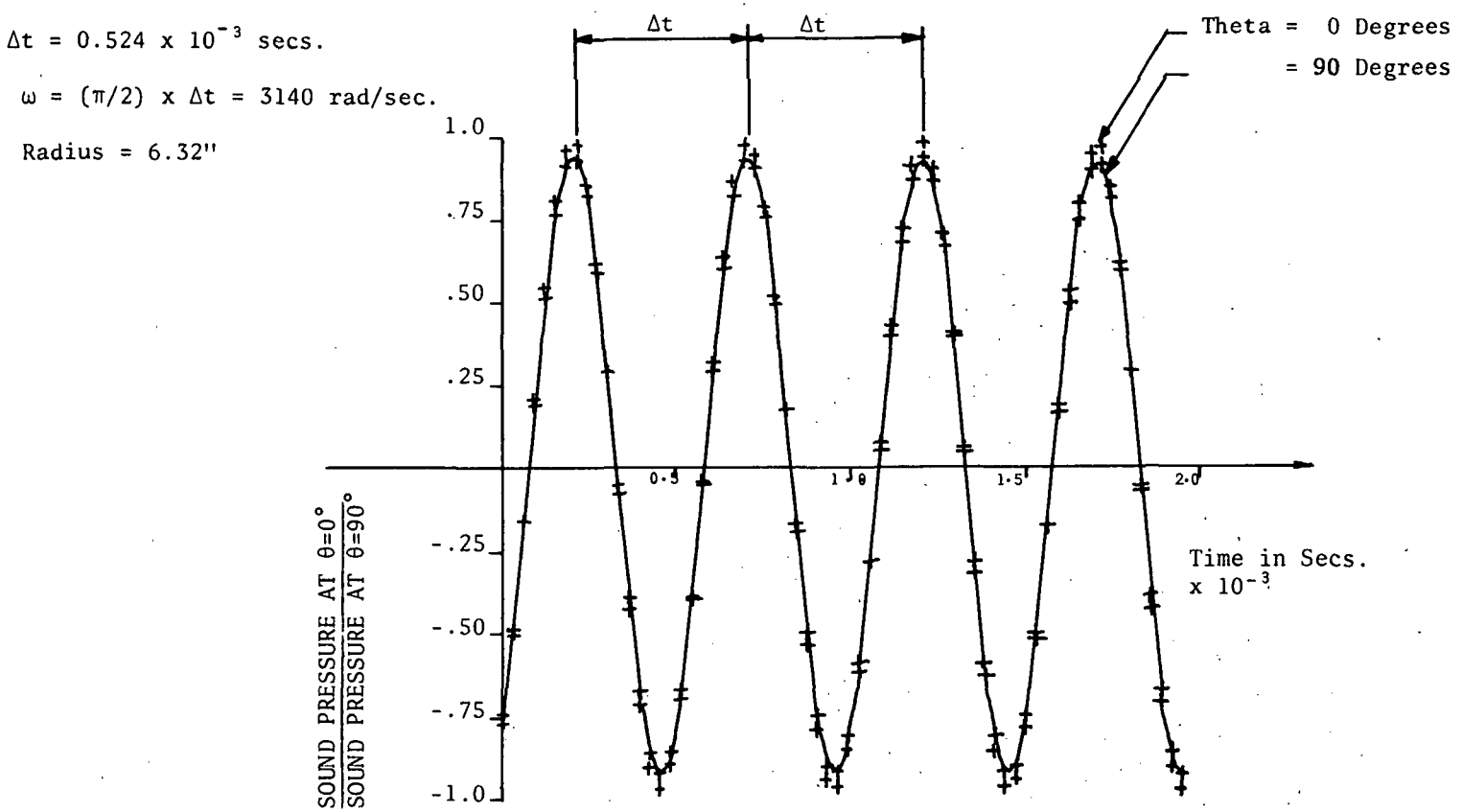

Figure 18 Calculated Sound Pressure vs. Time for Mode 4 at 2000 c/s.

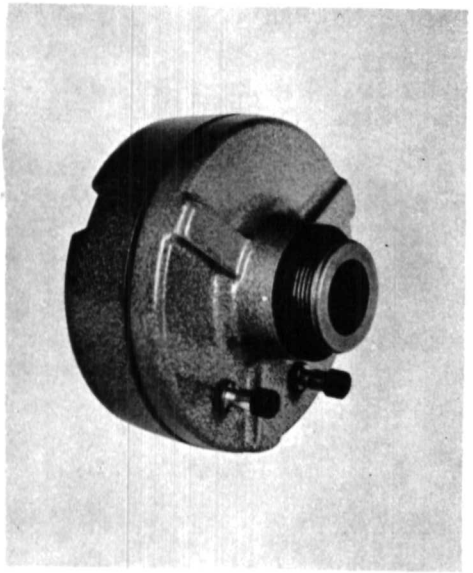

Sound Driver 1828-C

Frequency Response - 150 Hz - 10 kHz
Voice Coil Impedance - 8 Ohms
Power Handling Sine Wave - 20 Watts

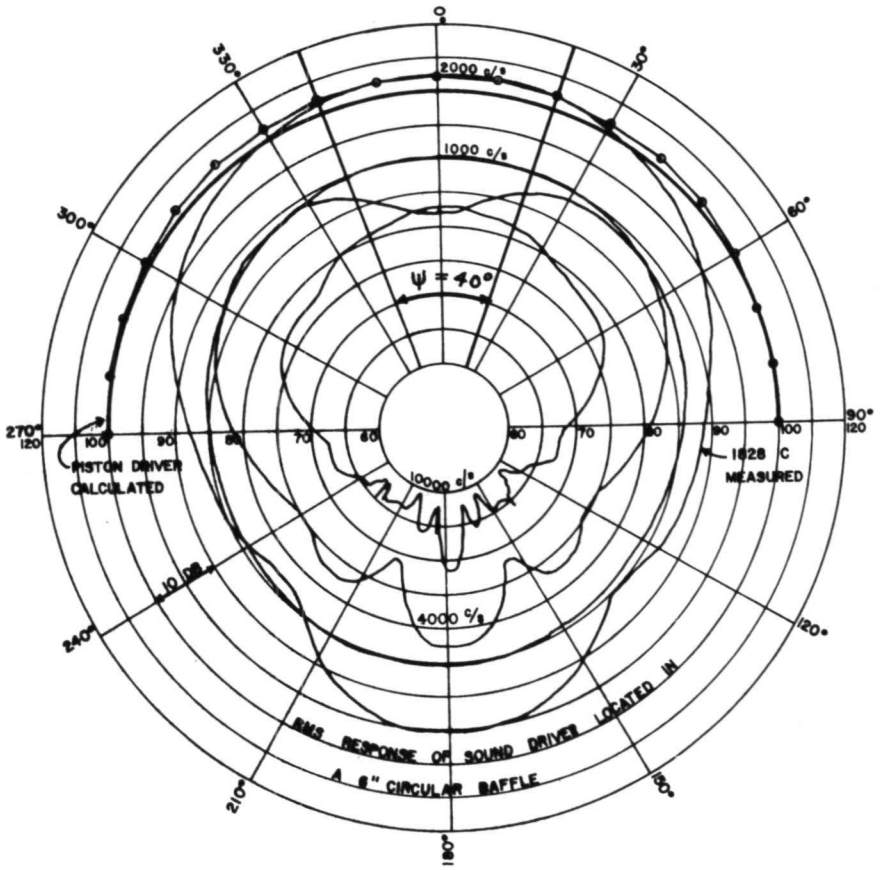

Figure 19 Comparison of 1828C and Piston Driver Radiation Patterns

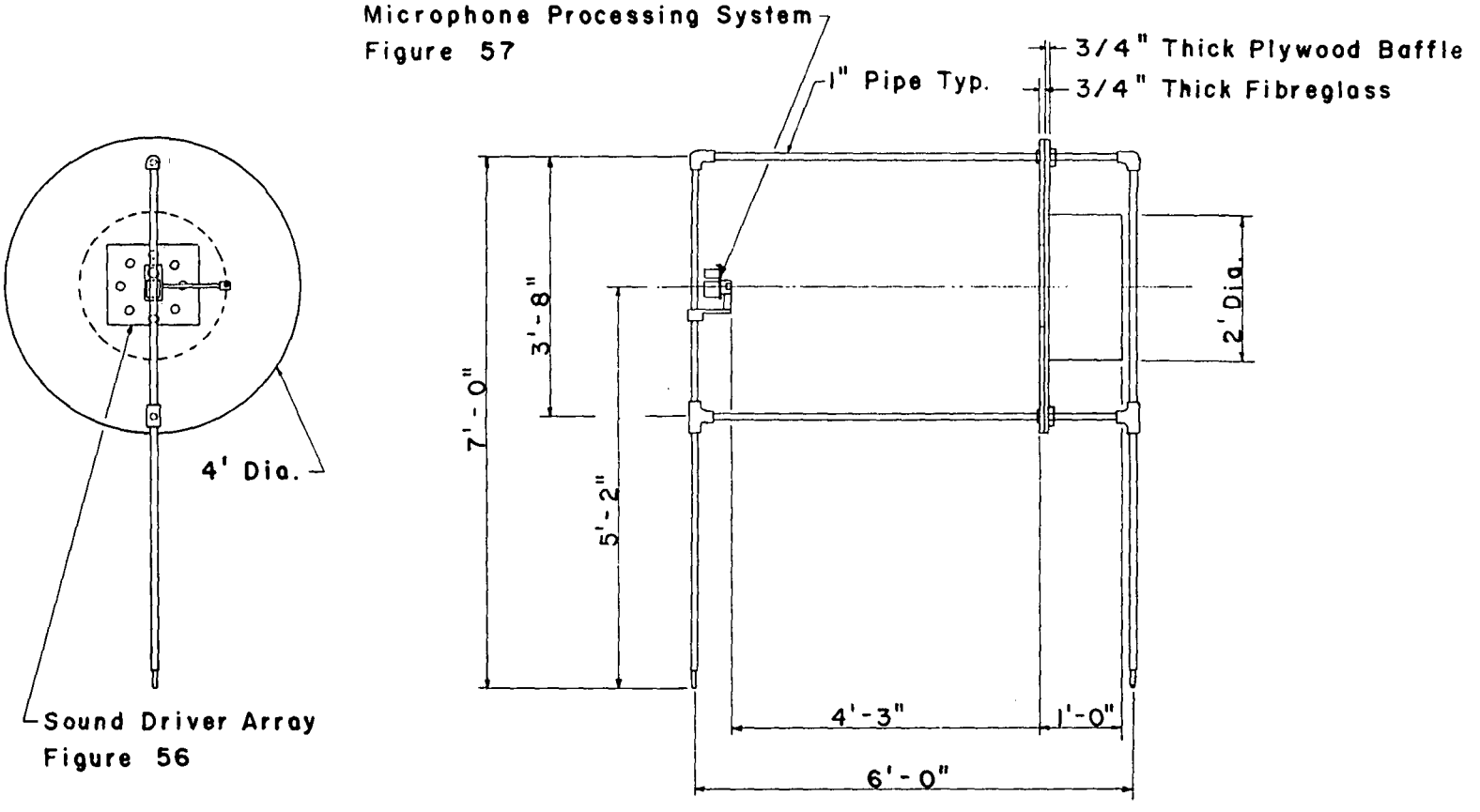

Figure 20 Assembly Drawing of Future Rig Fixtures

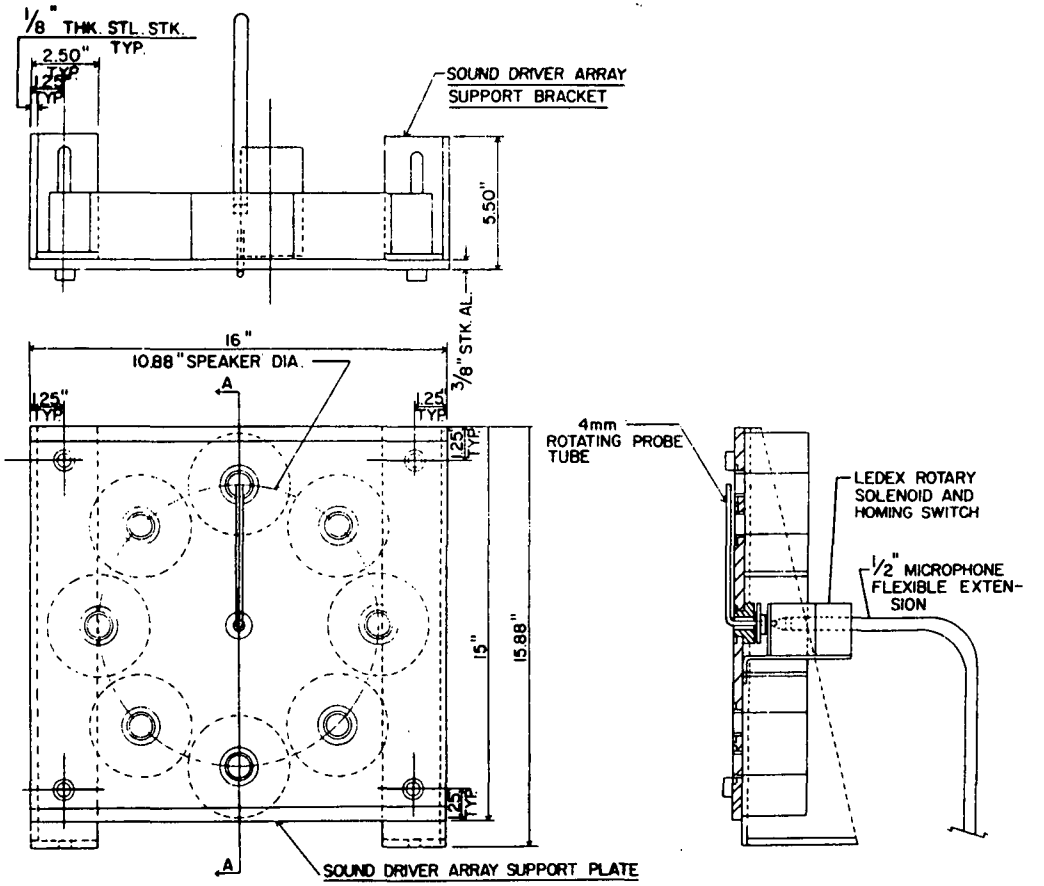

Figure 21 Assembly Drawing of Sound Driver Array and Support System

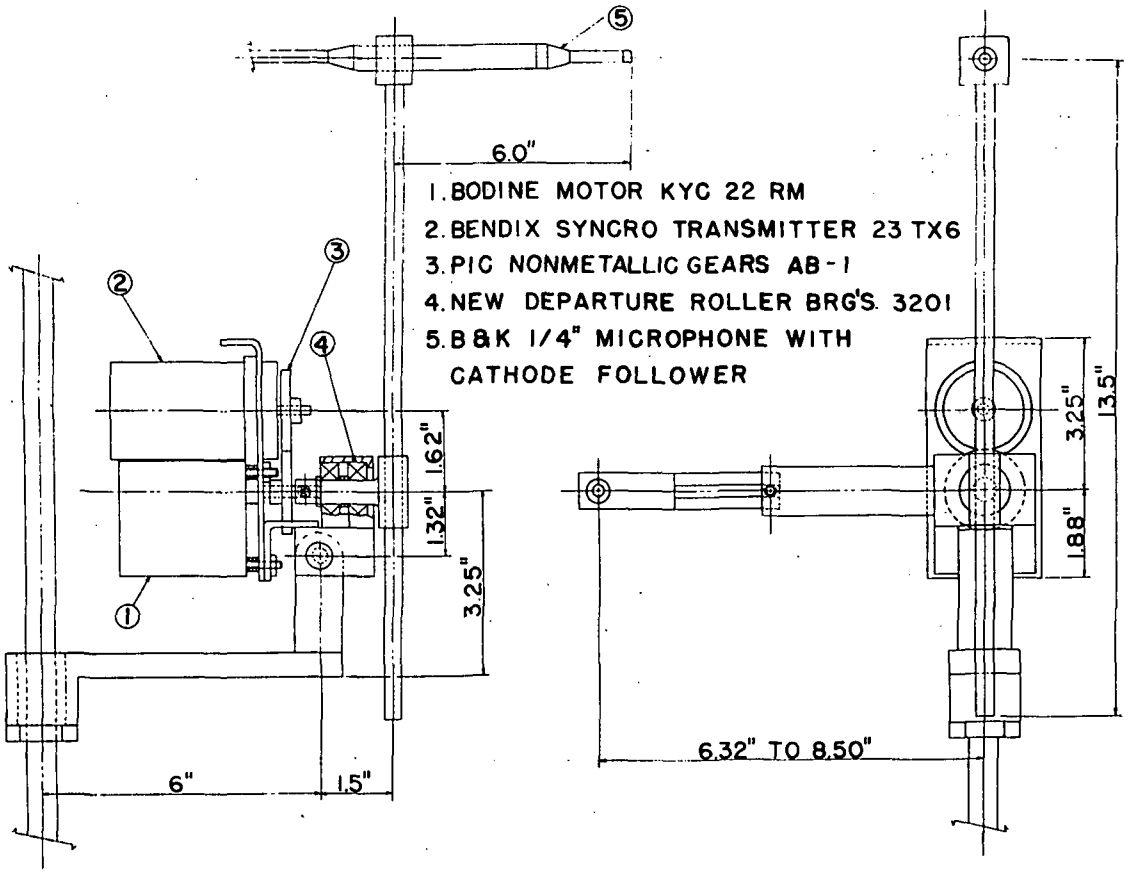

Figure 22 Assembly Drawing of 1/4" Microphone Sound Processing System

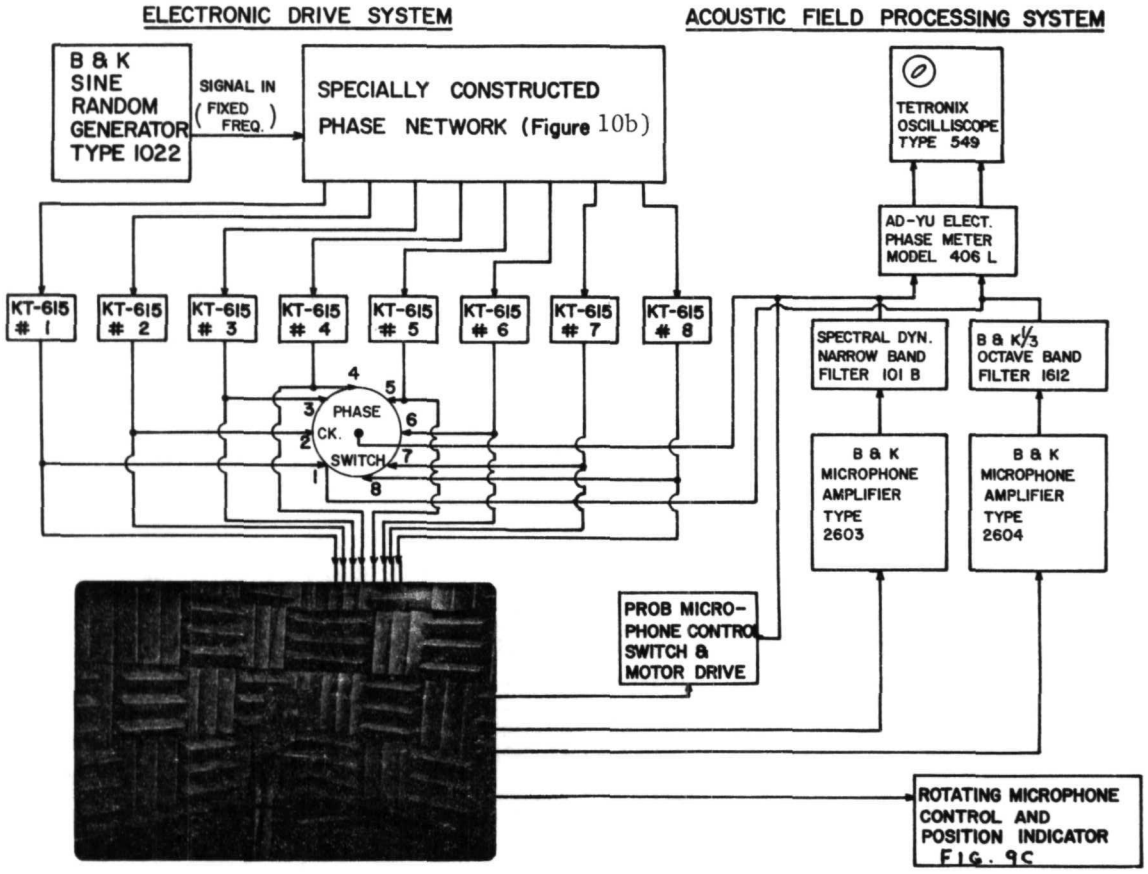

Figure 23 Equipment Schematic

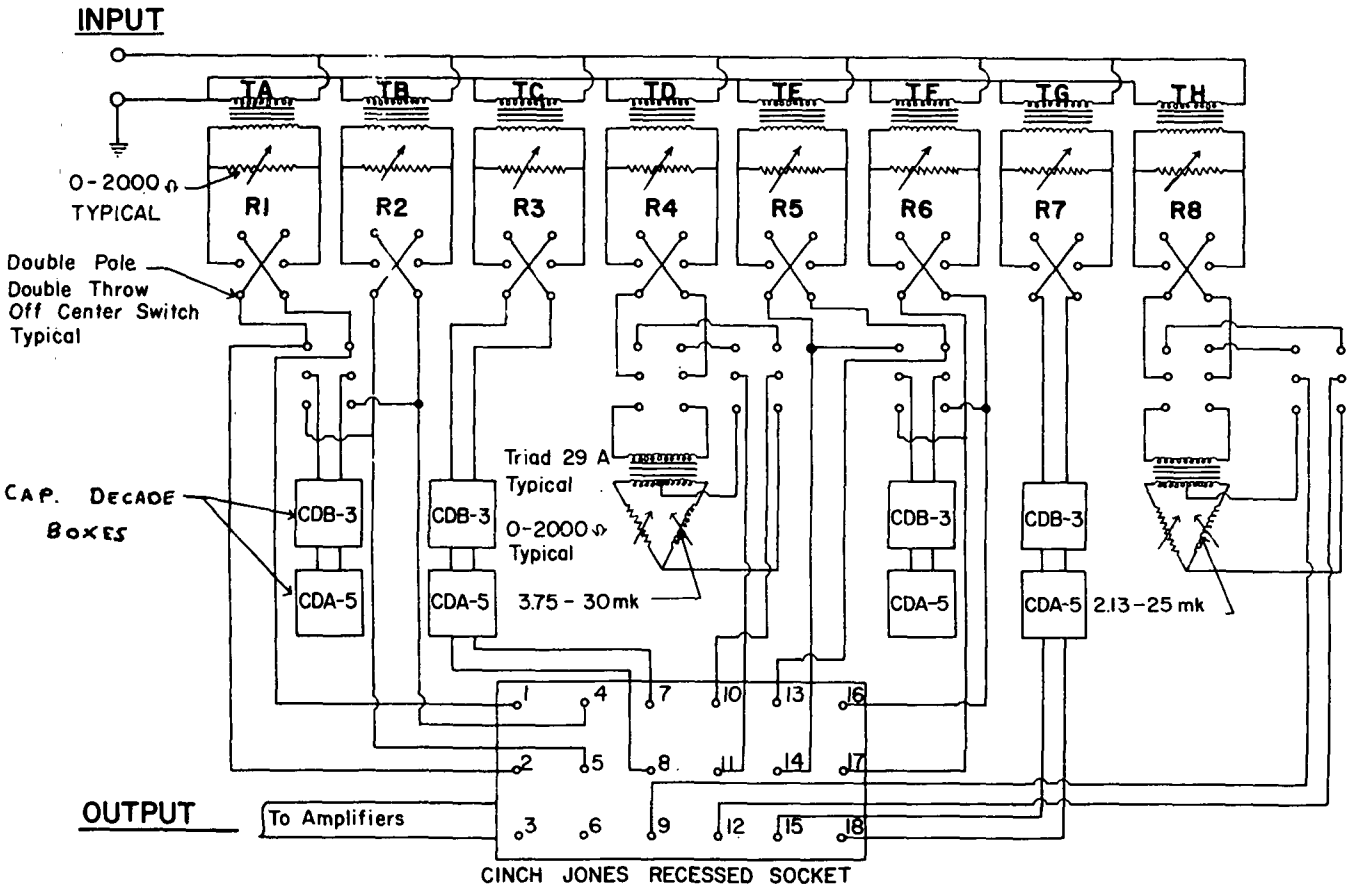

Figure 24 Phase Splitting Network

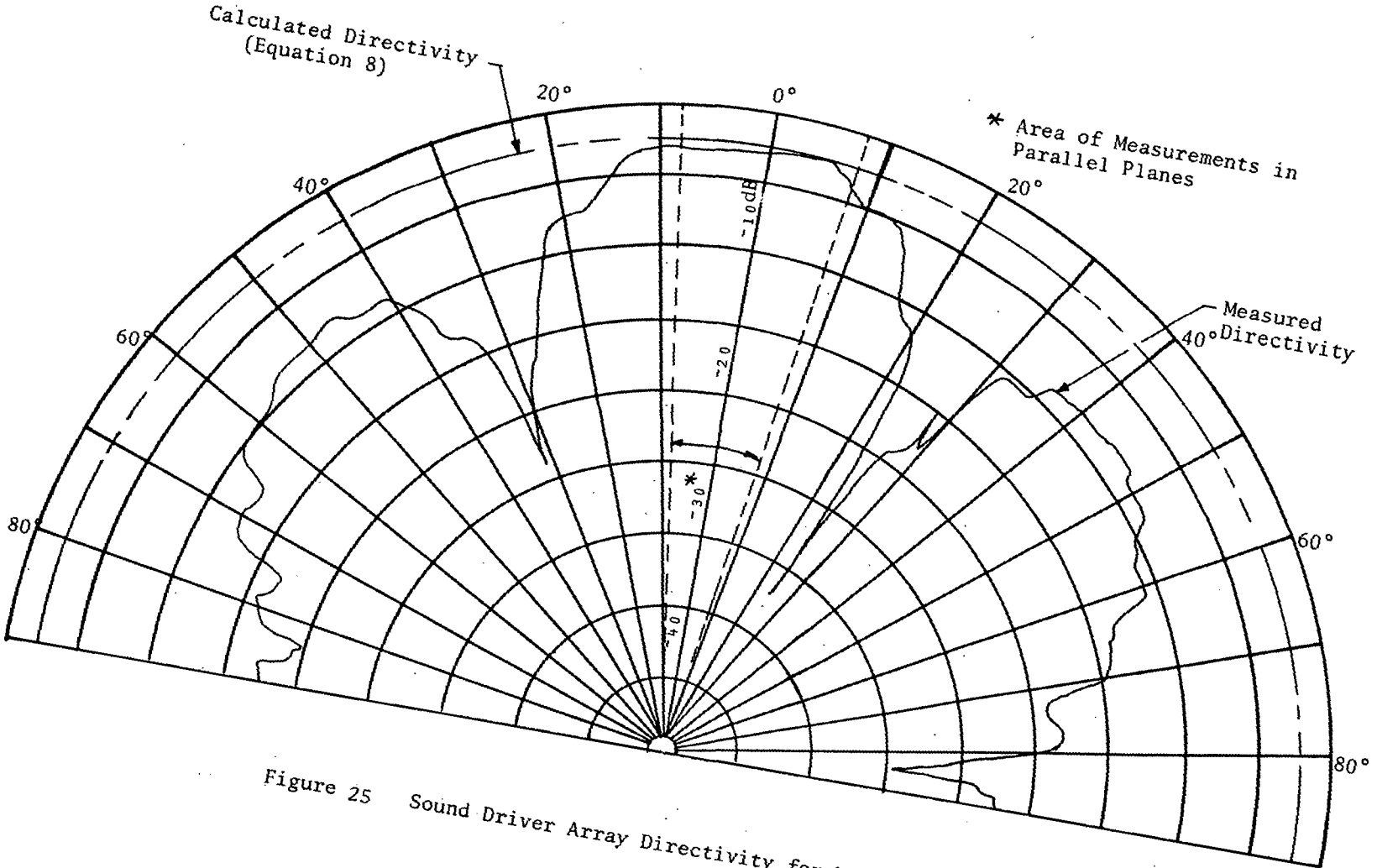

Figure 25 Sound Driver Array Directivity for Mode m=0 at 2000 c/s

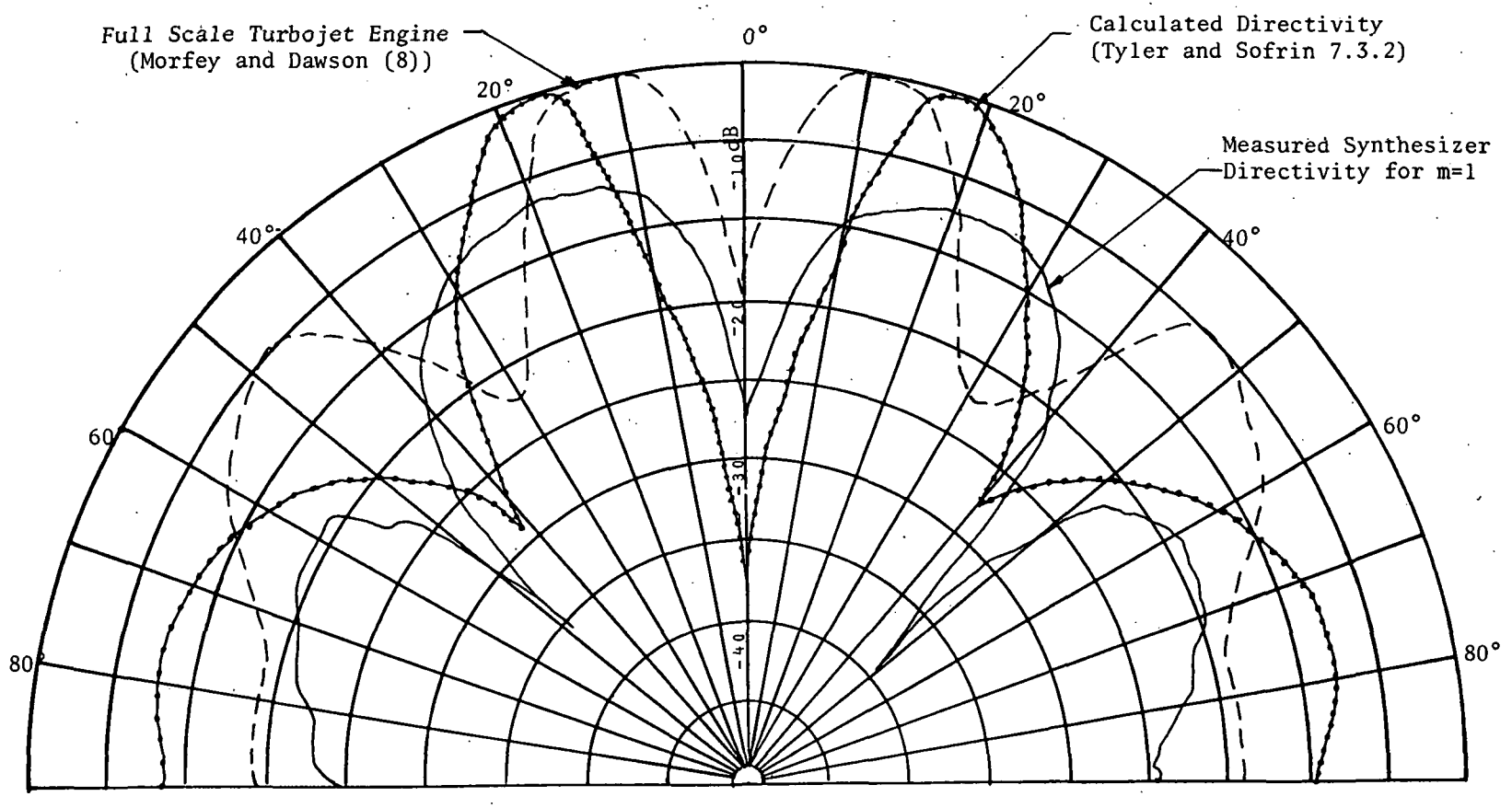

Figure 26 Sound Driver Array Directivity for Mode m=1 at 2000 c/s

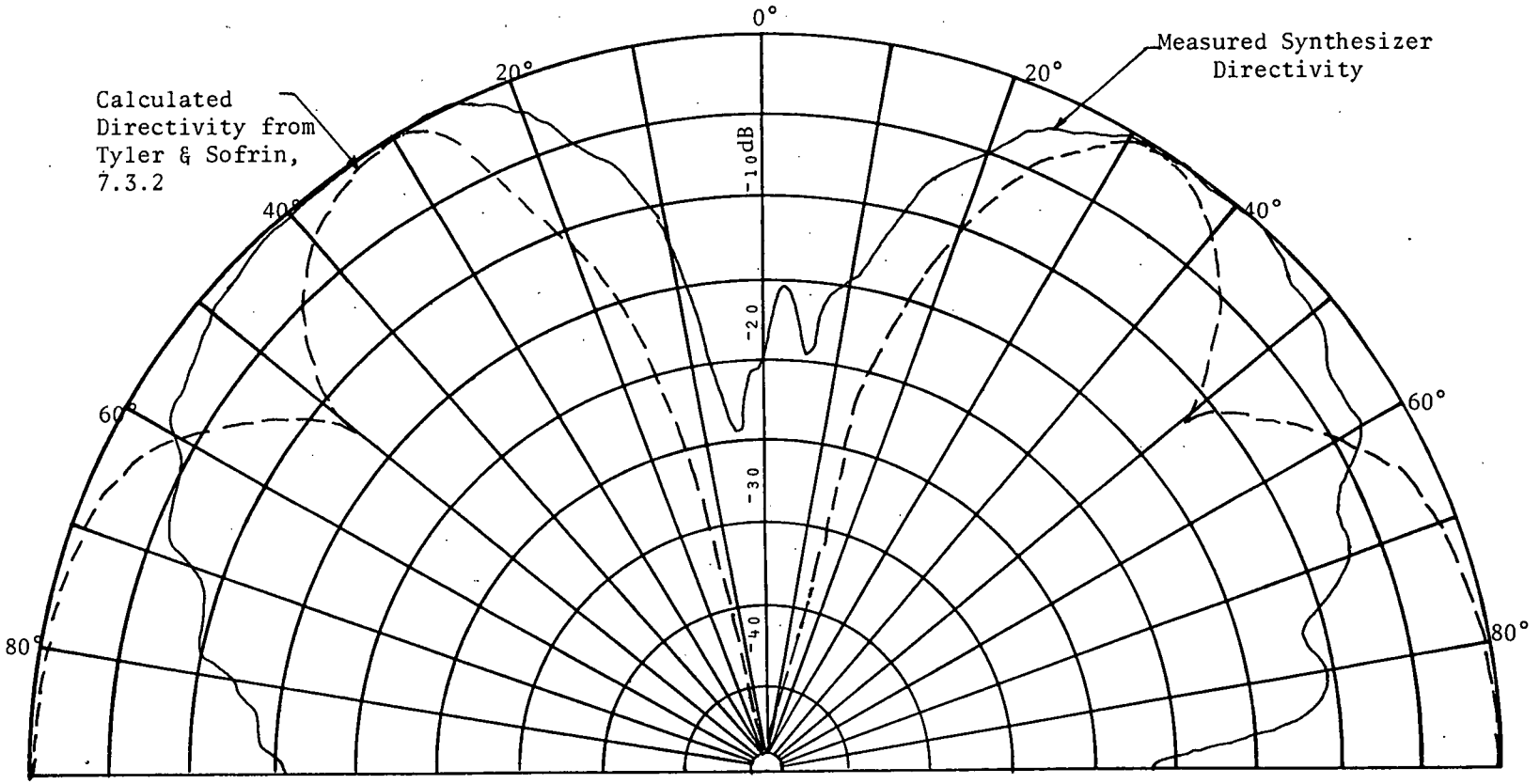

Figure 27 Sound Driver Array Directivity for Mode m=2 at 2000 c/s

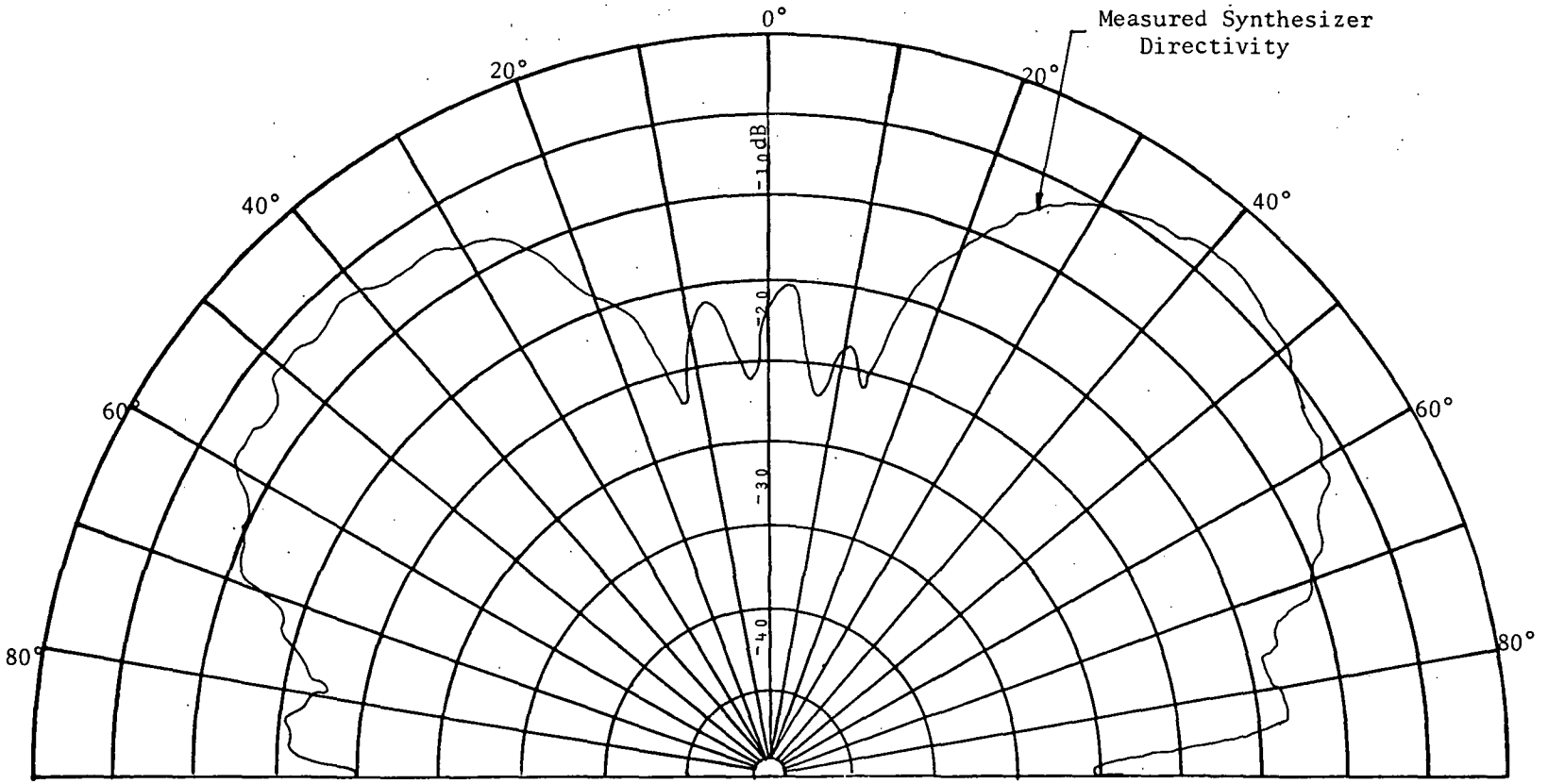

Figure 28 Sound Driver Array Directivity for Mode m=3 at 2000 c/s

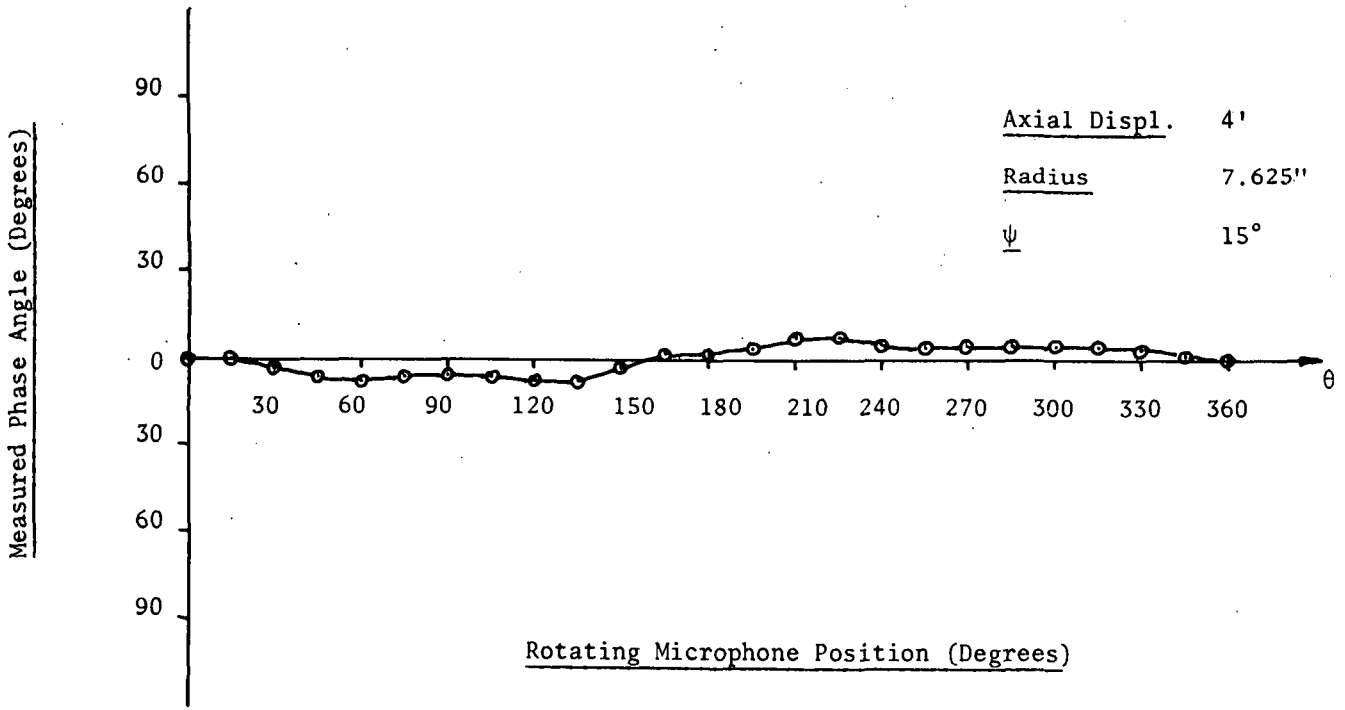

Figure 29 Measured Phase vs. Theta for Mode 0 at 2000 c/s

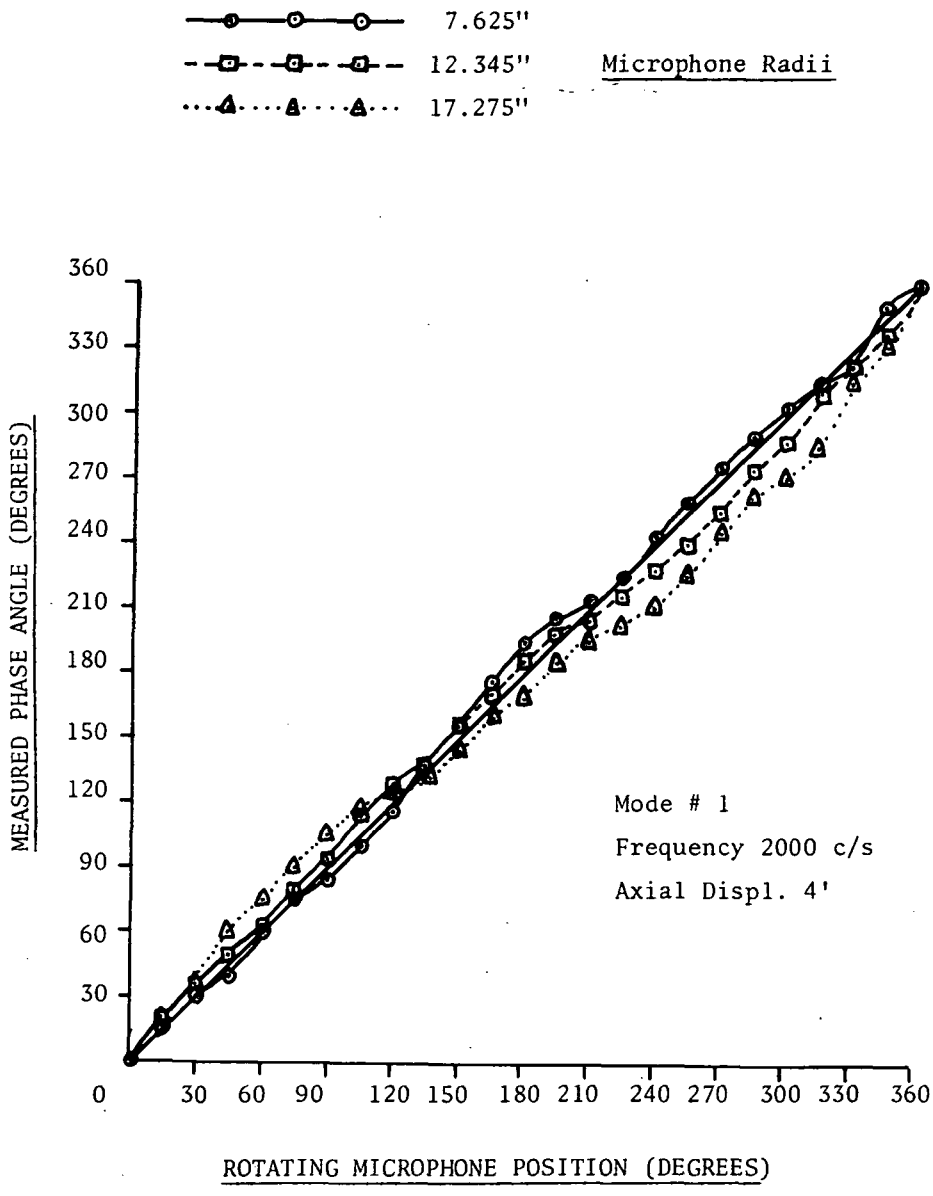

Figure 30 Measured Phase vs. Theta for Mode 1 at 2000 c/s.

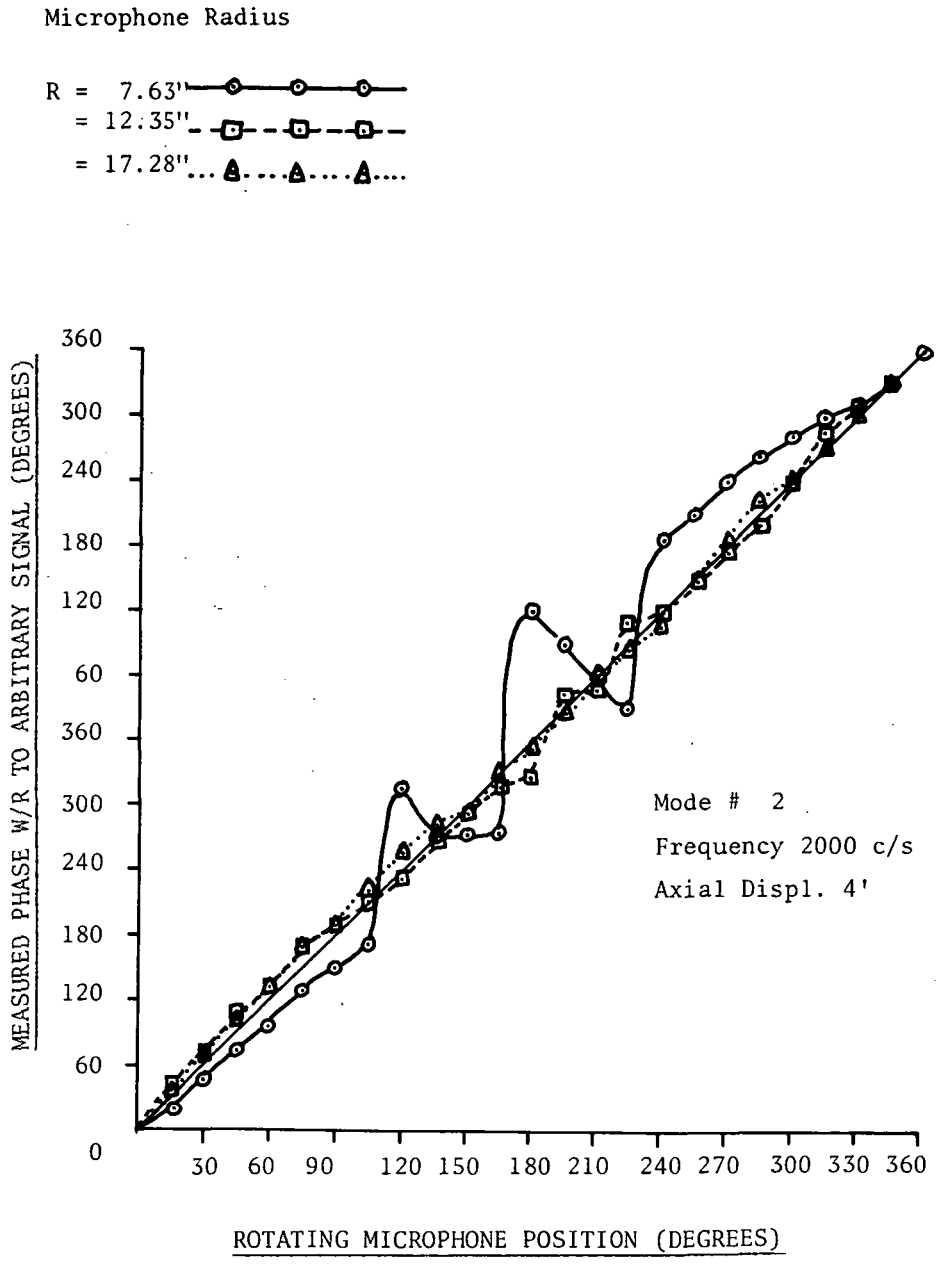

Figure 31 Measured Phase vs. Theta for Mode 2 at 2000 c/s

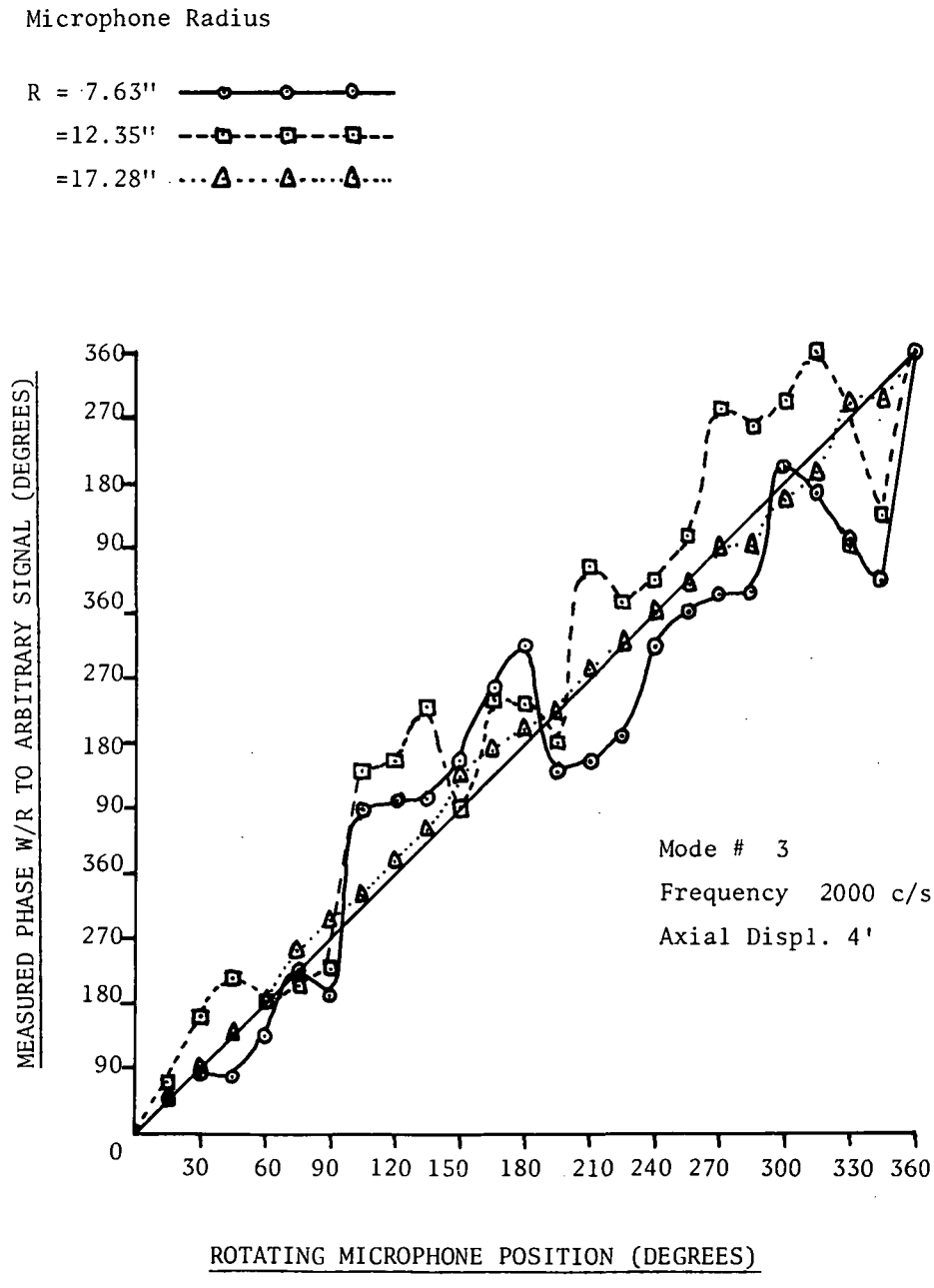

Figure 32 Measured Phase vs. Theta for Mode 3 at 2000 c/s.

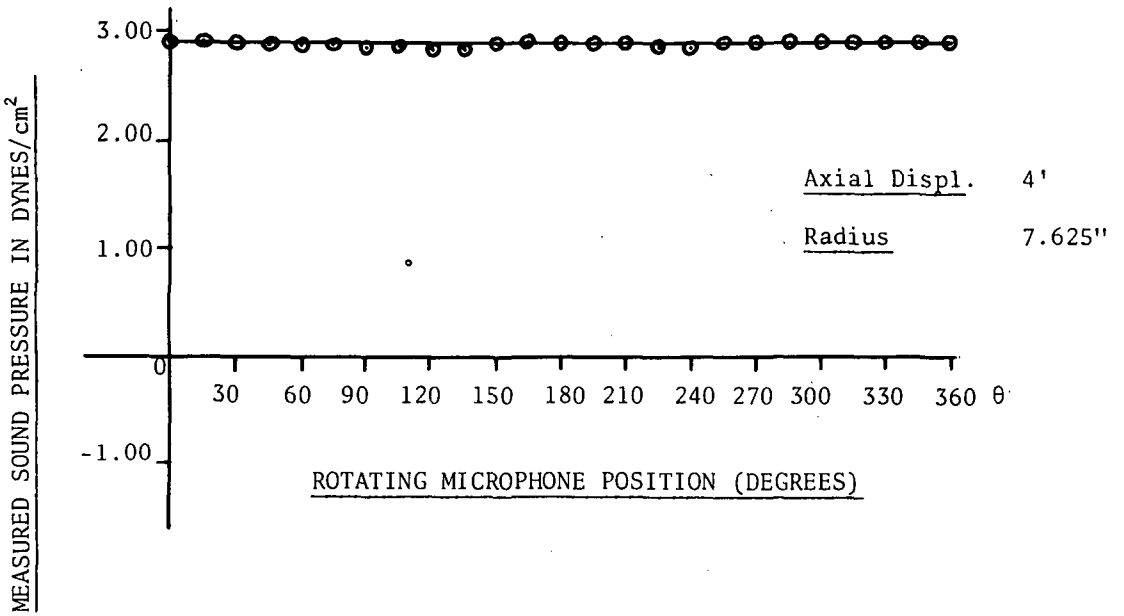

Figure 33 Measured Sound Pressure vs. Theta for Mode 0 at 2000 c/s.

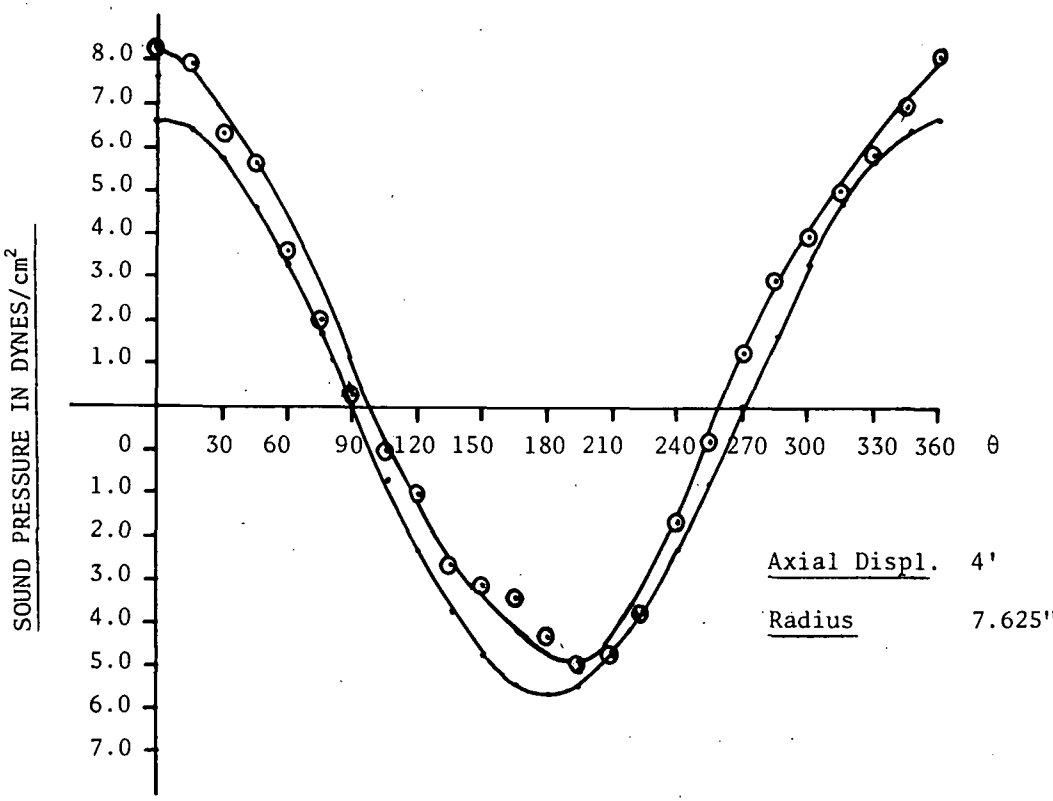

Figure 34 Measured Sound Pressure vs. θ for Mode 1 at 2000 c/s.

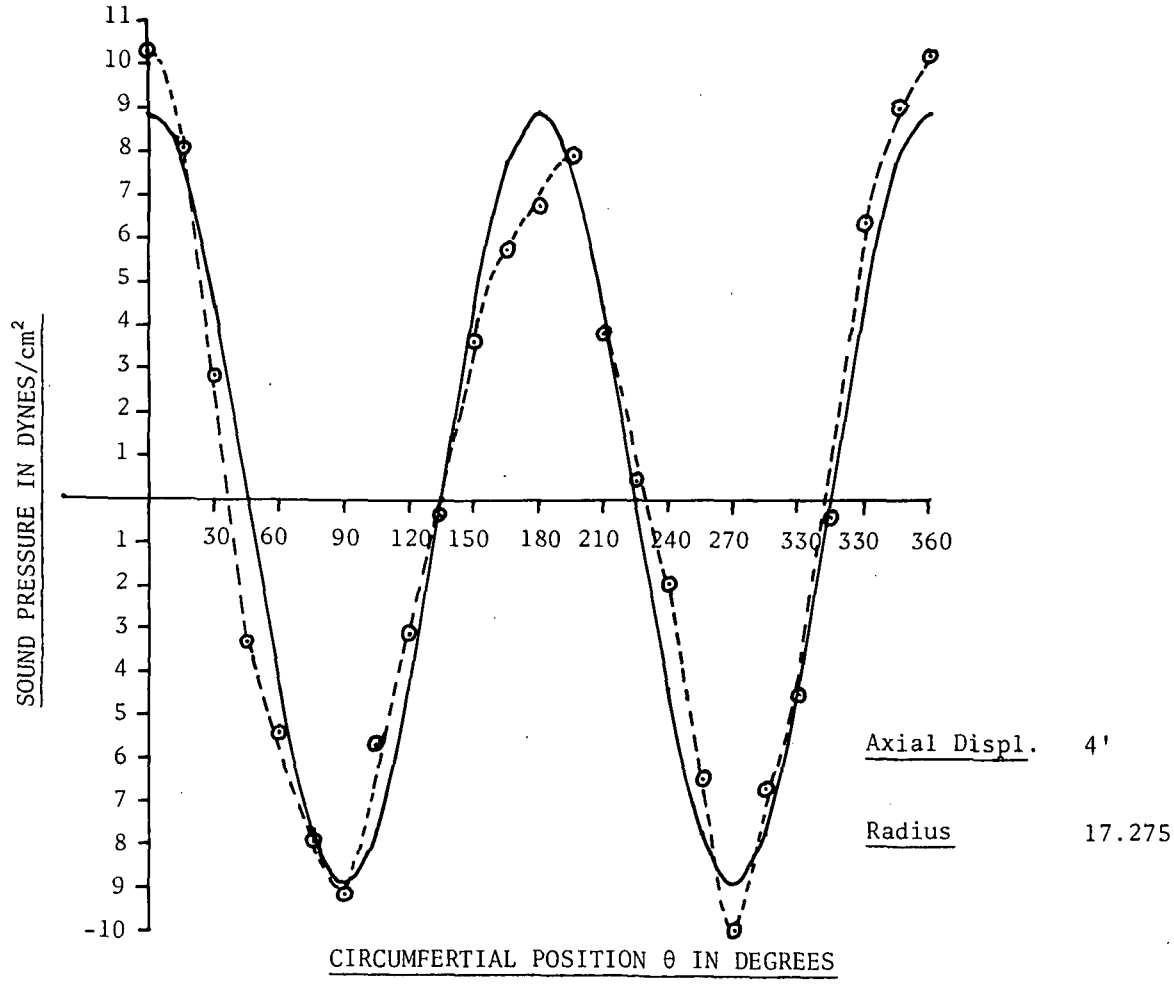

Figure 35 Measured Sound Pressure for a Fixed Time for Mode 2 at 2000 c/s.

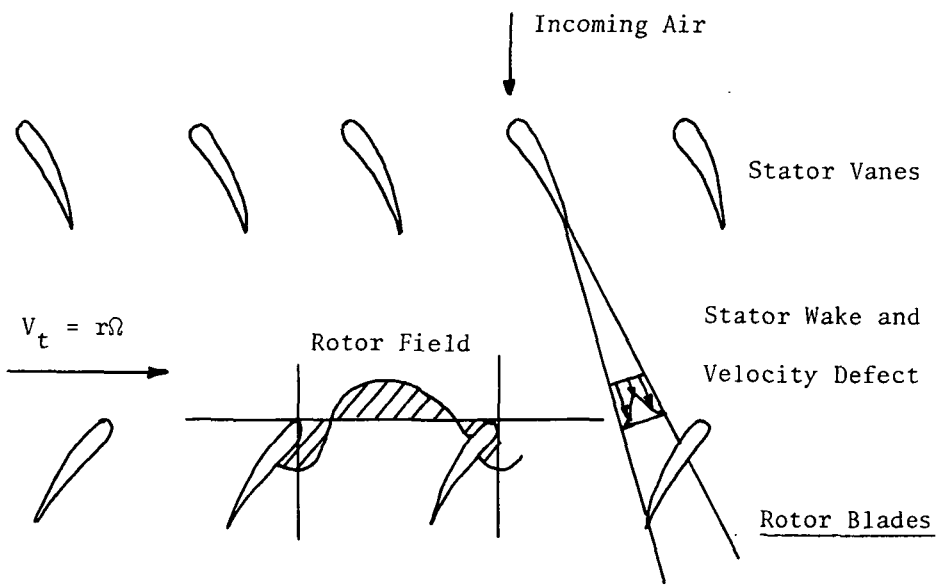

Schematic of Rotor-Stator Interaction

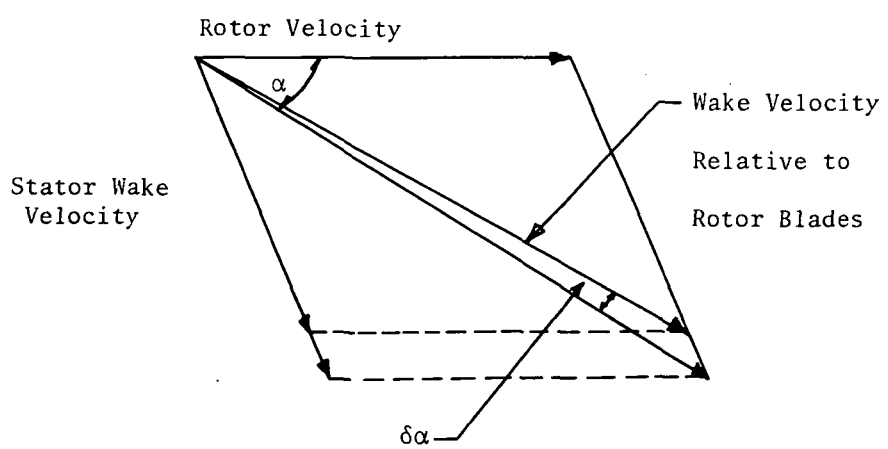

Velocity Triangles Indicating Fluctuating Air Angle

Figure B1 Schematic of Rotor-Stator Interaction (Lowson (6))

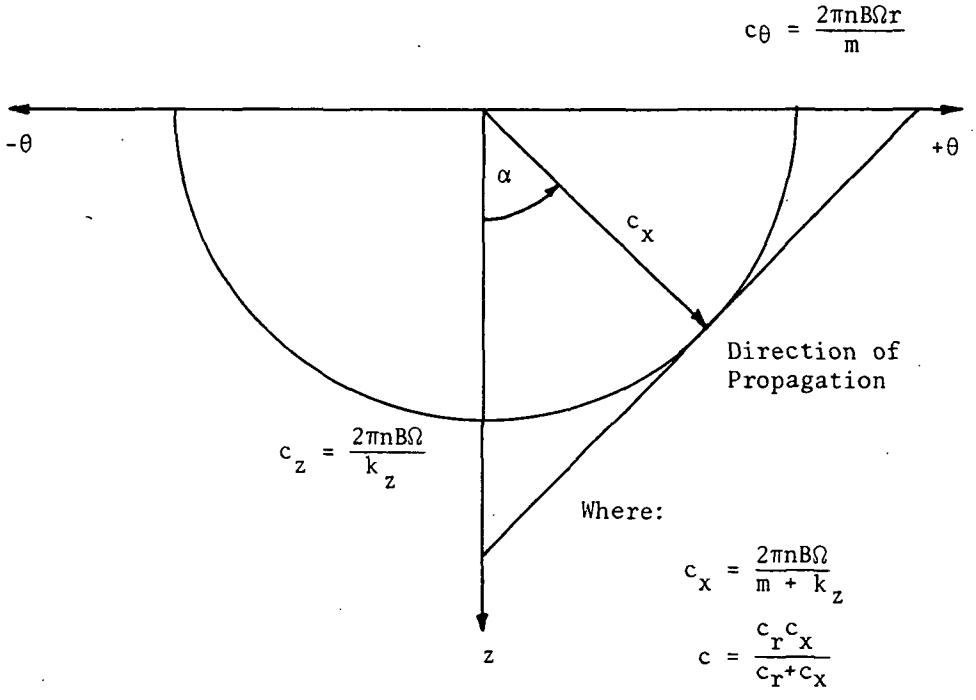

Figure B2 Property of a Propagating Wave

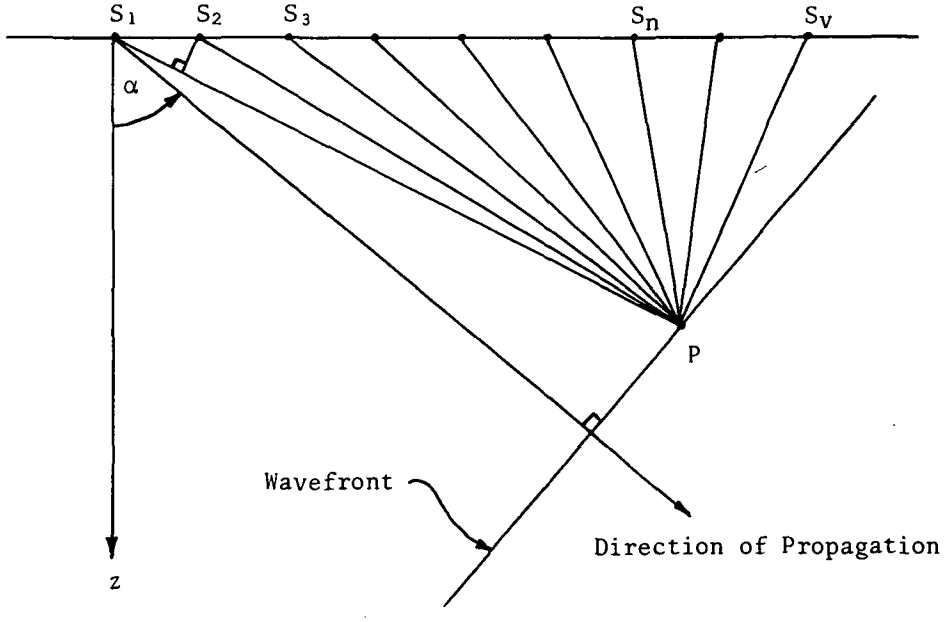

Figure B3 Radiation Due to Rotor-Stator Interaction

NASA-Langley, 1973 —— 2 CR-2260

NATIONAL AERONAUTICS AND SPACE ADMINISTRATION
WASHINGTON, D.C. 20546

OFFICIAL BUSINESS
PENALTY FOR PRIVATE USE $300

SPECIAL FOURTH-CLASS RATE
BOOK

POSTAGE AND FEES PAID
NATIONAL AERONAUTICS AND
SPACE ADMINISTRATION
451

U.S.MAIL

POSTMASTER: If Undeliverable (Section 158 Postal Manual) Do Not Return

"The aeronautical and space activities of the United States shall be conducted so as to contribute . . . to the expansion of human knowledge of phenomena in the atmosphere and space. The Administration shall provide for the widest practicable and appropriate dissemination of information concerning its activities and the results thereof."

—NATIONAL AERONAUTICS AND SPACE ACT OF 1958

NASA SCIENTIFIC AND TECHNICAL PUBLICATIONS

TECHNICAL REPORTS: Scientific and technical information considered important, complete, and a lasting contribution to existing knowledge.

TECHNICAL NOTES: Information less broad in scope but nevertheless of importance as a contribution to existing knowledge.

TECHNICAL MEMORANDUMS: Information receiving limited distribution because of preliminary data, security classification, or other reasons. Also includes conference proceedings with either limited or unlimited distribution.

CONTRACTOR REPORTS: Scientific and technical information generated under a NASA contract or grant and considered an important contribution to existing knowledge.

TECHNICAL TRANSLATIONS: Information published in a foreign language considered to merit NASA distribution in English.

SPECIAL PUBLICATIONS: Information derived from or of value to NASA activities. Publications include final reports of major projects, monographs, data compilations, handbooks, sourcebooks, and special bibliographies.

TECHNOLOGY UTILIZATION PUBLICATIONS: Information on technology used by NASA that may be of particular interest in commercial and other non-aerospace applications. Publications include Tech Briefs, Technology Utilization Reports and Technology Surveys.

Details on the availability of these publications may be obtained from:

SCIENTIFIC AND TECHNICAL INFORMATION OFFICE

NATIONAL AERONAUTICS AND SPACE ADMINISTRATION

Washington, D.C. 20546